

Bifurcations of a neural network model with symmetry

Ross Parker* and Andrea K. Barreiro†

Abstract. We analyze a family of clustered excitatory-inhibitory neural networks and the underlying bifurcation structures that arise because of permutation symmetries in the network as the global coupling strength g is varied. We primarily consider two network topologies: an all-to-all connected network which excludes self-connections, and a network in which the excitatory cells are broken into clusters of equal size. Although in both cases the bifurcation structure is determined by symmetries in the system, the behavior of the two systems is qualitatively different. In the all-to-all connected network, the system undergoes Hopf bifurcations leading to periodic orbit solutions; notably, for large g , there is a single, stable periodic orbit solution and no stable fixed points. By contrast, in the clustered network, there are no Hopf bifurcations, and there is a family of stable fixed points for large g .

Key words. dynamical systems, bifurcation theory, equivariant bifurcations, symmetry, neural networks

AMS subject classifications. 37C81, 37G10, 37G15, 92B20

1. Introduction. Today experimental techniques allow an increasingly detailed view of the physical architecture of biological neural networks. However, drawing a clear line from physical connectivity to dynamic neural activity is still a challenge. The networks in question are massive in scale and high dimensional (with billions of neurons and possibly trillions of synapse). Neural networks also show great diversity in structure at every level, from the morphology and excitability properties of a single cell to large scale connections between brain regions.

One common experimental finding is that neural dynamics are surprisingly low-dimensional when compared to the overall dimensionality of the neural system [16, 8, 18, 36, 27] (see Fig. 1 of [20] for a summary of earlier studies). The low-dimensional manifold may even shift slowly over time, as the underlying components of the network (cells and synapses) die and are replaced [19]. Thus, a major challenge for modern mathematical neuroscience is to understand how low-dimensional dynamics emerges from the observed connectivity of the brain.

Real neural networks are partially structured but also partially random. Intuitively, it's clear that not every connection in the brain must be tuned precisely (after all, every person reading this sentence will respond to these black markings in the same way, despite significant differences between our individual brains). This has motivated the use of analytical tools of random network theory, in which one seeks to draw conclusions about an ensemble of networks. An early example is the work by Sompolinsky et al. [35] which applies dynamic mean field theory to single-population firing-rate networks in which connections are chosen from a mean-zero Gaussian distribution: in the limit of large network size, the authors find that the network transitions from quiescence to chaos as a global coupling parameter passes a bifurcation value. This value coincides with the point at which the spectrum of the connectivity matrix exits the unit circle [22, 3] thus making the connection to random matrix theory very concrete. Later authors have sought to extend these results to correlated or block-structured matrices [28, 2], and many others have studied the spectral characteristics of partially structured connection matrices [37, 1, 31] with neural networks as a primary motivation.

However, the results of spectral theory and nonlinear dynamics have not always neatly aligned. One network setting that has caused persistent difficulty is excitatory-inhibitory networks with strong average connections [32]. The predictions of random matrix theory suggest chaotic, asyn-

*Department of Mathematics, Southern Methodist University, Dallas, TX (rhparker@smu.edu).

†Department of Mathematics, Southern Methodist University, Dallas, TX (abarreiro@smu.edu).

chronous fluctuations, whereas large-scale coherent fluctuations have been observed instead. Why? The answer may be found in the nature of the deterministic perturbation. Several authors have examined how low-rank, asymmetric perturbations create an effectively feed-forward structure that allows coherent dynamics to co-exist with random fluctuations in an orthogonal subspace [13, 12, 30, 29]; the dimensionality of the dynamical subspace can be related to the dimension of the low-rank perturbation in the connectivity matrix [34, 5].

In an earlier work, we found an alternative possibility [4]. In examining balanced E-I networks without self-coupling, we persistently observed periodic solutions which could not be explained by random matrix theory. Instead, they arose as a consequence of underlying symmetries in the connection matrix and could be predicted through the machinery of equivariant bifurcation theory. However, some pieces of our analysis remained uncompleted: we were unable at that time to give a complete stability analysis. This is important because the stable solution is what one can expect to observe in a perturbed (random) network.

Here, we complete this analysis for all-to-all excitatory-inhibitory networks. We then extend this analysis to a biologically significant block-structured case, in which the excitatory cells are clustered, but inhibition is global. We find that the dynamics are strikingly different: instead of limit cycles, we predict fixed points. In both cases, the structures can be understood by considering the symmetries of the deterministic connection matrix.

2. Mathematical model. We consider a network in which each node represents the firing rate of a single neuron. The individual neurons are connected by sigmoidal activation functions through a connectivity matrix, which specifies both the network of neuronal connections and the weight of each connection, including whether a given neuron is excitatory (E) or inhibitory (I). With noise in the connectivity matrix, this is an idealized model in neuroscience [21, 32, 28]. Here, we will consider the system without noise, but where the connection weights have important symmetries. Specifically, we study:

$$\dot{\mathbf{x}} = F(\mathbf{x}, g) := -\mathbf{x} + \frac{1}{\sqrt{N}} H \tanh(g\mathbf{x}), \quad (2.1)$$

for $\mathbf{x} \in \mathbb{R}^N$, where the global coupling strength, g , is used a bifurcation parameter. The network comprises a total of N neurons, of which n_E are excitatory and n_I are inhibitory. H is the $N \times N$ connectivity matrix; the diagonal entries of H are all 0 to exclude self-interactions of neurons (see [4, Sec. 2.1] for a discussion on why self-coupling of neurons is removed). We will use the parameter $f = n_E/N$ to identify the fraction of neurons that are excitatory: for the remainder of this paper we will use $f = 0.8$ for a 4-to-1 excitatory-to-inhibitory ratio, which is typical for cortical networks [7]. We note that F is an odd function of \mathbf{x} , i.e. $F(-\mathbf{x}) = -F(\mathbf{x})$. This implies that if $\mathbf{x}(t)$ is a solution to (2.1), so is $-\mathbf{x}(t)$, and that $\mathbf{x} = \mathbf{0}$ is a fixed point of (2.1) for all g .

We consider here networks in which the excitatory neurons are grouped into n_C clusters, each containing p neurons, and the inhibitory neurons are grouped into n_{C_I} clusters, each containing p_I neurons. In addition, all connections of any given type (e.g. $E \rightarrow E$ or $E \rightarrow I$) will have the same

strength. The matrix H then takes the general form

$$H = \left[\begin{array}{cccc|cccc} \mu_{EE}\mathbf{K}_p & 0 & \dots & 0 & & & & \\ 0 & \mu_{EE}\mathbf{K}_p & \dots & 0 & & & & \\ \vdots & \vdots & \ddots & 0 & & & & \\ 0 & 0 & \dots & \mu_{EE}\mathbf{K}_p & & & & \\ \hline & & & & \mu_{II}\mathbf{K}_{pI} & 0 & \dots & 0 \\ & & & & 0 & \mu_{II}\mathbf{K}_{pI} & \dots & 0 \\ & & & & \vdots & \vdots & \ddots & 0 \\ & & & & 0 & 0 & \dots & \mu_{II}\mathbf{K}_{pI} \end{array} \right], \quad (2.2)$$

where $\mathbf{1}_{m \times n}$ is the $m \times n$ matrix of ones, and \mathbf{K}_n is the $n \times n$ matrix with all ones off the diagonal, i.e. $\mathbf{K}_n = \mathbf{1}_{n \times 1}(\mathbf{1}_{n \times 1})^T - \mathbf{I}_n$, with \mathbf{I}_n the $n \times n$ identity matrix. The connection weights μ are defined “matrix-style”, e.g. μ_{EI} will denote the connection from I to E, while μ_{IE} will denote the connection from E to I. The weights are also signed, so that $\mu_{EE}, \mu_{IE} > 0$ and $\mu_{EI}, \mu_{II} < 0$: this reflects the neurobiological heuristic of *Dale’s Law*, which states that each neuron makes excitatory or inhibitory connections onto its postsynaptic targets.

The linearization of (2.1) about $\mathbf{x} = 0$ is the matrix

$$DF(0) = \frac{g}{\sqrt{N}}H - I_N, \quad (2.3)$$

where I_N is the $N \times N$ identity matrix. The eigenvalues of $DF(0)$ are then given by $\lambda^*(g) = \frac{g}{\sqrt{N}}\lambda - 1$ for all eigenvalues λ of H . As a consequence, the dynamics of the system can be understood in terms of the eigenvalues of H . (See Figure 2.1 for the eigenvalue pattern of H of the three network models we will discuss below). For an eigenvalue λ of H with negative real part, the corresponding eigenvalue $\lambda^*(g)$ of $DF(0)$ will always have negative real part, irrespective of g . On the other hand, for an eigenvalue λ of H with positive real part, the sign of the real part of the corresponding eigenvalue $\lambda^*(g)$ of $DF(0)$ will depend on the bifurcation parameter g . Thus, the only bifurcations of $\mathbf{x} = 0$ involve the eigenvalues of H which have positive real part. Furthermore, the multiplicities of the eigenvalues of H are determined by symmetries in the underlying model (2.1) and the matrix H . These lead to symmetric bifurcations as g is varied.

The dynamics near a nonzero fixed point $\mathbf{x}^* = (x_1^*, \dots, x_N^*)^T$ of (2.1) also depend on the matrix H . The linearization of (2.1) about \mathbf{x}^* is the matrix

$$DF(\mathbf{x}^*) = \frac{g}{\sqrt{N}}H(\mathbf{x}^*) - I_N, \quad (2.4)$$

where

$$H(\mathbf{x}^*) := H \text{diag}(\text{sech}^2(g\mathbf{x}^*)) \quad (2.5)$$

is obtained from the matrix H by multiplying column j of H by $\text{sech}^2(gx_j^*)$. We note that the diagonal entries of $H(\mathbf{x}^*)$ are 0, thus $\text{Trace } H(\mathbf{x}^*) = 0$. This implies that the eigenvalues of $H(\mathbf{x}^*)$ sum to 0.

Features of the system such as fixed points and periodic orbits remain when the connectivity matrix is perturbed by a random matrix, i.e. $G = H + \epsilon A$ for small ϵ , even when the spectrum of G bears no obvious resemblance to the original spectrum of H . We first reported on this phenomenon in [4], where we analyzed all-to-all connected, balanced excitatory-inhibitory networks ($n_C = 1$ and $n_{CI} = 1$). In this paper, we first flesh out some details about that system: we derive leading order

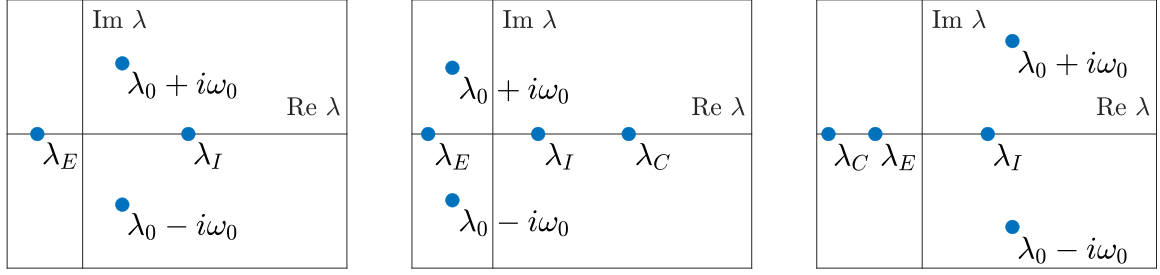


Figure 2.1. Eigenvalue pattern of the connectivity matrix H for different configurations studied in this paper. Left: single excitatory and single inhibitory cluster [section 4](#). Middle: multiple excitatory clusters and single inhibitory cluster [section 5](#). Right: single excitatory cluster and multiple inhibitory clusters [section 6](#). The notation for the eigenvalues in each network model is explained in the corresponding section below.

expressions for bifurcation points in the system, for the equilibria near those bifurcation points, and for the Hopf bifurcations that spawn the clustered limit cycles we observed in [\[4\]](#) ([section 4](#)). We then extend the analysis to networks in which the excitatory population is split up into clusters ($n_C > 1, n_{C_I} = 1$; [section 5](#)). We briefly compare with networks in which the inhibitory neurons are clustered instead ($n_C = 1, n_{C_I} > 1$; [section 6](#)).

3. Model simplification. Since our main interest is locating fixed points and periodic orbits, we can simplify the model using the fact that all excitatory cells within each excitatory cluster must be synchronized at a fixed point or periodic orbit. In the case where there is a single excitatory cluster ($n_C = 1$), if x_1 and x_2 are the activities of two excitatory cells, then a straightforward calculation (see Lemma 3 from [\[4\]](#)) shows that

$$\frac{d}{dt}|x_1 - x_2|^2 \leq -2|x_1 - x_2|^2. \quad (3.1)$$

The only way this can be true for a fixed point (for which $\frac{d}{dt}|x_1 - x_2|^2 = 0$) or for a periodic orbit (for which $x_1(t) - x_2(t) = x_1(t+T) - x_2(t+T)$ for some period T) is if $x_1(t) = x_2(t)$ for all t . If $n_C > 1$, and x_1 and x_2 are the activities of two cells in the same excitatory cluster, equation [\(3.1\)](#) holds by the same argument as in [\[4\]](#), since both neurons receive the same incoming connections with the same weights.

We are primarily interested in the case where there is a single cluster of inhibitory cells ($n_{C_I} = 1$). We will briefly consider the case of multiple excitatory inhibitory ($n_{C_I} > 1$) in [section 6](#). If there are n_C excitatory clusters containing p cells each, and n_I inhibitory cells (for $N = pn_C + n_I$ total cells), equation [\(2.1\)](#) reduces to the system of $n_C + n_I$ equations

$$\begin{aligned} \dot{x}_{E_j} &= -x_{E_j} + \frac{(p-1)}{\sqrt{N}}\mu_{EE}\tanh(gx_{E_j}) + \frac{1}{\sqrt{N}}\mu_{EI}\sum_k \tanh(gx_{I_k}) \quad j = 1, \dots, n_C \\ \dot{x}_{I_j} &= -x_{I_j} + \frac{p}{\sqrt{N}}\mu_{IE}\sum_k \tanh(gx_{E_k}) + \frac{1}{\sqrt{N}}\mu_{II}\sum_{k \neq j} \tanh(gx_{I_k}) \quad j = 1, \dots, n_I, \end{aligned} \quad (3.2)$$

where x_{E_j} is the activity for the j th excitatory cluster, and x_{I_j} is activity for the j th inhibitory cell. In matrix form, the equations [\(3.2\)](#) can be written

$$\dot{\mathbf{x}} = \tilde{F}(\mathbf{x}, g) := -\mathbf{x} + \frac{1}{\sqrt{N}}\tilde{H}\tanh(g\mathbf{x}), \quad (3.3)$$

where $\mathbf{x} = (x_{E_1}, \dots, x_{E_{n_C}}, x_{I_1}, \dots, x_{I_{n_I}})^T$, and \tilde{H} is the $(n_C + n_I) \times (n_C + n_I)$ reduced matrix

$$\tilde{H} = \left[\begin{array}{c|c} (p-1)\mu_{EE}I_{n_C} & \mu_{EI}\mathbf{1}_{n_C \times n_I} \\ \hline p\mu_{IE}\mathbf{1}_{n_I \times n_C} & \mu_{II}\mathbf{K}_{n_I} \end{array} \right]. \quad (3.4)$$

Let $\mathbf{x}^* = (x_{E_1}^*, \dots, x_{E_{n_C}}^*, x_{I_1}^*, \dots, x_{I_{n_I}}^*)^T$ be a fixed point of (3.3). The linearization of (3.3) about \mathbf{x}^* is the matrix

$$D\tilde{F}(\mathbf{x}^*) = \frac{g}{\sqrt{N}}\tilde{H}(\mathbf{x}^*) - I_{n_C+n_I}, \quad (3.5)$$

where

$$\tilde{H}(\mathbf{x}^*) := \tilde{H} \text{diag}(\text{sech}^2(g\mathbf{x}^*)). \quad (3.6)$$

The original equation (2.1) has a corresponding fixed point \mathbf{x}_0^* , in which each $x_{E_j}^*$ in \mathbf{x}^* is repeated p times. The following proposition shows that to analyze the stability of the fixed point \mathbf{x}_0^* in the full system (2.1), it suffices to determine the eigenvalues of the reduced matrix $\tilde{H}(\mathbf{x}^*)$, since the additional eigenvalues of $H(\mathbf{x}_0^*)$ are negative, and thus will not affect stability.

Proposition 3.1. *Let \mathbf{x}^* be a fixed point of (3.3) and \mathbf{x}_0^* the corresponding fixed point of (2.1), and let $H(\mathbf{x}_0^*)$ and $\tilde{H}(\mathbf{x}^*)$ be defined by (2.5) and (3.6). Then*

(i) *Every eigenvalue of $\tilde{H}(\mathbf{x}^*)$ is an eigenvalue of $H(\mathbf{x}_0^*)$.*

(ii) *$H(\mathbf{x}_0^*)$ has n_C additional real, negative eigenvalues, each with multiplicity $p-1$.*

Proof. For part (i), let $\mathbf{v} = (v_{E_1}, \dots, v_{E_{n_C}}, v_{I_1}, \dots, v_{I_{n_I}})^T$ be an eigenvector of $\tilde{H}(\mathbf{x}^*)$ with eigenvalue λ . By comparing $\tilde{H}(\mathbf{x}^*)$ and $H(\mathbf{x}_0^*)$, there is a corresponding eigenvector \mathbf{v}_0 to $H(\mathbf{x}_0^*)$ with the same eigenvalue λ , where \mathbf{v}_0 is obtained from \mathbf{v} by repeating each entry v_{E_j} p times. For part (ii), it can be verified directly that for $j = 1, \dots, n_C$, $H(\mathbf{x}_0^*)$ has an eigenvalue at $\lambda = -\mu_{EE} \text{sech}^2(x_{E_j})$ with multiplicity $p-1$. For $j = 1$, for example, the $p-1$ eigenvectors are $\mathbf{v}^1, \dots, \mathbf{v}^{p-1}$, where $v_1^k = -1$, $v_{k+1}^k = 1$, and all other components are 0. Since $\mu_{EE} > 0$, these eigenvalues are always negative. ■

4. Single excitatory and inhibitory cluster. The simplest case (considered in [4]) involves a single excitatory cluster ($n_C = 1$) and a single inhibitory cluster ($n_{CI} = 1$), in which case the matrix H in (2.1) reduces to

$$H = \left[\begin{array}{c|c} \mu_{EE}\mathbf{K}_{n_E} & \mu_{EI}\mathbf{1}_{n_E \times n_I} \\ \hline \mu_{IE}\mathbf{1}_{n_I \times n_E} & \mu_{II}\mathbf{K}_{n_I} \end{array} \right].$$

We choose the connection weights so that the network is *balanced*; that is, the excitatory and inhibitory currents coming into each cell should approximately cancel [32]. To achieve this balance, we set $\mu_{EI} = -\alpha\mu_{EE}$ and $\mu_{II} = -\alpha\mu_{IE}$, where $\alpha = \frac{f}{1-f}$. For simplicity, we also take $\mu_{IE} = \mu_{EE}$. The spectrum of H is now easy to compute [4]. The eigenvalues of H (left panel of Figure 2.1) are

- $\lambda_I := \alpha\mu_{EE} > 0$ with multiplicity $n_I - 1$.
- $\lambda_E := -\mu_{EE} < 0$ with multiplicity $n_E - 1$.

- One complex pair of eigenvalues $\lambda_0 \pm i\omega_0$, with

$$\lambda_0 := \mu_{EE} \frac{\alpha - 1}{2}, \quad \omega_0 := \mu_{EE} \sqrt{\alpha + 1} \sqrt{n_E - \frac{\alpha + 1}{4}}.$$

It is straightforward to check that $\lambda_E < 0 < \lambda_0 < \lambda_I$. As discussed above, all bifurcations of $\mathbf{x} = 0$ involve only $\lambda_0 \pm i\omega_0$ and λ_I , which are the eigenvalues of H with positive real part.

In the following sections, we will determine the bifurcations which occur as g is increased, together with the structures which emerge at these bifurcation points. First, the origin loses stability in a symmetric pitchfork bifurcation, after which point there is a branch of equilibria for every possible division of the inhibitory cells into two groups. We will derive leading order formulas for these branches, as well as show which of them are initially stable. As g is further increased, there is a Hopf bifurcation on each of these branches, which gives rise to a limit cycle with the same grouping pattern as the corresponding branch. Finally, at a critical values of g , these limit cycles coalesce in a symmetric pitchfork bifurcation of limit cycles. After this point, there is a single stable limit cycle in which there is one group of inhibitory cells and one group of excitatory cells.

4.1. Bifurcations of the origin. As the bifurcation parameter g is increased from 0, the eigenvalue $\lambda_I^*(g)$ of $DF(0)$ corresponding to λ_I crosses the imaginary axis at

$$g = g_0 := \frac{\sqrt{N}}{\alpha \mu_{EE}}. \quad (4.1)$$

The origin $\mathbf{x} = 0$ is a stable equilibrium for $g < g_0$. At $g = g_0$, the origin loses stability in a symmetric pitchfork bifurcation, where $n_I - 1$ eigenvalues cross the imaginary axis simultaneously (see [subsection 4.2](#) below). As g is further increased, the complex pair of eigenvalues $\lambda_0^*(g) \pm i\omega_0^*(g)$ of $DF(0)$ crosses the imaginary axis at

$$g = g_H := \frac{2\sqrt{N}}{(\alpha - 1)\mu_{EE}}, \quad (4.2)$$

at which point a Hopf bifurcation occurs, giving rise to a limit cycle (see [subsection 4.5](#) below). The frequency of this limit cycle is given by the imaginary part $\omega_0^*(g)$ at $g = g_H$, which is

$$\omega_0^*(g_H) = \frac{2}{\alpha - 1} \sqrt{\alpha + 1} \sqrt{fN - \frac{\alpha + 1}{4}}, \quad (4.3)$$

where we used $n_E = fN$. We note that since $\omega_0^*(g_H) = \mathcal{O}(\sqrt{N})$, $\omega_0^*(g_H) \rightarrow \infty$ as $N \rightarrow \infty$.

4.2. Solutions after symmetric pitchfork bifurcation. Our main tool for analyzing the solutions to (2.1) which arise at bifurcation points when symmetries are present is the *Equivariant Branching Lemma* [10, 23, 26]. Before stating this result, we introduce some terminology. Let Γ be a finite group acting on \mathbb{R}^N ; then we say that a mapping $F : \mathbb{R}^N \rightarrow \mathbb{R}^N$ is Γ -equivariant if $F(\gamma\mathbf{x}) = \gamma F(\mathbf{x})$, for all $\mathbf{x} \in \mathbb{R}^N$ and $\gamma \in \Gamma$. A one-parameter family of mappings $F : \mathbb{R}^N \times \mathbb{R} \rightarrow \mathbb{R}^N$ is Γ -equivariant, if it is Γ -equivariant for each value of its second argument. We say that V , a subspace of \mathbb{R}^N , is Γ -invariant if $\gamma\mathbf{v} \in V$, for any \mathbf{v} and $\gamma \in \Gamma$. We furthermore say that the action of Γ on V is *irreducible* if V has no proper invariant subspaces, i.e. the only Γ -invariant subspaces of V are $\{0\}$ and V itself.

For a group Γ and a vector space V , we define the *fixed-point subspace* for Γ , denoted $\text{Fix}(\Gamma)$, to be all points in V that are unchanged under any of the members of Γ , i.e. $\text{Fix}(\Gamma) = \{\mathbf{x} \in V : \gamma\mathbf{x} = \mathbf{x}, \forall \gamma \in \Gamma\}$. The *isotropy subgroup* of $\mathbf{x} \in V$, denoted $\Sigma_{\mathbf{x}}$, is the set of all members of Γ

under which \mathbf{x} is fixed, i.e. $\Sigma_{\mathbf{x}} = \{\gamma \in \Gamma : \gamma\mathbf{x} = \mathbf{x}\}$. We then say that a subgroup Σ is an isotropy subgroup of Γ , if it is the isotropy subgroup, $\Sigma_{\mathbf{x}}$, for some $\mathbf{x} \in V$.

Suppose we have a one-parameter family of mappings, $F(\mathbf{x}, g)$, and we wish to solve $F(\mathbf{x}, g) = 0$. For any $(\mathbf{x}, g) \in \mathbb{R}^n \times \mathbb{R}$, let $(dF)_{\mathbf{x},g}$ denote the $N \times N$ Jacobian matrix

$$\left[\frac{\partial F_j}{\partial x_k}(\mathbf{x}, g) \right]_{j,k=1\dots N}$$

A bifurcation will occur when the Jacobian ceases to be invertible, i.e. when $(dF)_{\mathbf{x},g}$ has a nontrivial kernel. For a Γ -equivariant mapping — i.e. $F(\mathbf{x}, g)$ is Γ -equivariant for any value of the parameter g — we may have *multiple* eigenvalues go through zero at once, because of symmetries; however, the structural changes that occur are qualitatively the same as those that occur in a non-symmetric system in which a single eigenvalue crosses through zero. Furthermore, we will have *multiple* such solution branches, each corresponding to a subgroup of the original symmetries. This is formalized in the following theorem:

Theorem 4.1 (Equivariant Branching Lemma: paraphrased from [23], pg. 82, see also pg. 67-69). *Let $F : \mathbb{R}^N \times \mathbb{R} \rightarrow \mathbb{R}^N$ be a one-parameter family of Γ -equivariant mappings with $F(\mathbf{x}_0, g_0) = \mathbf{0}$. Suppose that (\mathbf{x}_0, g_0) is a bifurcation point and that, defining $V = \ker(dF)_{\mathbf{x}_0, g_0}$, Γ acts absolutely irreducibly on V . Let Σ be an isotropy subgroup of Γ satisfying*

$$\dim \text{Fix}(\Sigma) = 1, \tag{4.4}$$

where $\text{Fix}(\Sigma)$ is the fixed-point subspace of Σ : that is, $\text{Fix}(\Sigma) \equiv \{\mathbf{x} \in V \mid \sigma\mathbf{x} = \mathbf{x}, \forall \sigma \in \Sigma\}$. Then there exists a unique smooth solution branch to $F = 0$ such that the isotropy subgroup of each solution is Σ .

The reader can readily check that the right-hand side of (2.1) is Γ -equivariant, for $\Gamma = S_{n_E} \times S_{n_I}$, where S_n is the group of permutations on n objects. That is, we can permute the labels on the excitatory cells, and/or the labels on the inhibitory cells, without changing the equations.

At $g = g_0$, $n_I - 1$ eigenvalues pass through zero: the corresponding eigenspace is the set of all zero-sum vectors with support in the inhibitory cells only; i.e.

$$V \equiv \ker(dF)_{\mathbf{0}, g^*} = \text{span} \left\{ \left[\begin{array}{c} 0 \quad \cdots \quad 0 \quad \mathbf{v}_{n_I} \\ \underbrace{\hspace{1.5cm}}_{n_E} \end{array} \right] \right\}, \quad \mathbf{v}_{n_I} \perp \mathbf{1}_{n_I}.$$

To check that Γ acts irreducibly on V it is sufficient to show that the subspace spanned by the *orbit* of a single vector \mathbf{v} (defined as the set of all values $\gamma\mathbf{v}$, for $\gamma \in \Gamma$) is full rank; this can be readily confirmed for $\mathbf{v}_{n_I} = [1 \quad -1 \quad 0 \quad \dots \quad 0]$, for example.

To find the appropriate subgroup of symmetries, we break the inhibitory cells up into precisely two clusters and retain only permutations within each cluster. This describes a subgroup of Γ , $\Sigma = S_{n_E} \times S_{n_{I_1}} \times S_{n_{I_2}}$, $n_{I_1} + n_{I_2} = n_I$. Assuming that (without loss of generality) the I_1 neurons have the indices $n_E + 1, \dots, n_E + n_{I_1}$, and so forth, Σ has the fixed point subspace

$$\text{Fix}(\Sigma) = \text{span} \left\{ \left[\begin{array}{c} 0 \quad \cdots \quad 0 \quad 1 \quad \cdots \quad 1 \quad -\frac{n_{I_1}}{n_{I_2}} \quad \cdots \quad -\frac{n_{I_1}}{n_{I_2}} \\ \underbrace{\hspace{1.5cm}}_{n_E} \quad \underbrace{\hspace{1.5cm}}_{n_{I_1}} \quad \underbrace{\hspace{1.5cm}}_{n_{I_2}} \end{array} \right] \right\}. \tag{4.5}$$

We can check that $\text{Fix}(\Sigma)$ is a subspace of V . Furthermore $\dim \text{Fix}(\Sigma) = 1$ because it can be described as the span of a single vector.

As a consequence, there is a branch of equilibria emerging at the symmetric pitchfork bifurcation point $g = g_0$ for every possible division of the inhibitory cells into exactly two clusters of size n_{I_1} and n_{I_2} , where $n_{I_1} + n_{I_2} = n_I$. We refer to these as I_1/I_2 branches. Each such branch may be characterized by the number $\beta = n_{I_1}/n_{I_2}$, which gives the ratio of the cluster sizes. Without loss of generality, we may take $n_{I_1} \geq n_{I_2}$, so that $\beta \geq 1$. The inhibitory cells within each of the two clusters are synchronized. The solution on each I_1/I_2 branch is then given as (x_E, x_{I_1}, x_{I_2}) , where we recall from [section 3](#) that all excitatory cells are synchronized. Due to the odd symmetry of [\(2.1\)](#), there is a corresponding I_1/I_2 branch for each β with solution $(-x_E, -x_{I_1}, -x_{I_2})$. We will ignore this other branch for simplicity, although we note that it is this odd symmetry which permits a pitchfork bifurcation to occur.

4.3. Solutions along I_1/I_2 branches. First, we derive leading order expressions for the equilibria along the I_1/I_2 branches for g close to the bifurcation point g_0 . Fix $\beta \geq 1$. To find (x_E, x_{I_1}, x_{I_2}) along the I_1/I_2 branch corresponding to β , we reduce [\(3.2\)](#) to the 3-dimensional system

$$\begin{bmatrix} x_E \\ x_{I_1} \\ x_{I_2} \end{bmatrix} = \frac{\mu_{EE}}{\sqrt{N}} \begin{bmatrix} (\alpha n_I - 1) & -\alpha \frac{\beta}{\beta+1} n_I & -\alpha \frac{1}{\beta+1} n_I \\ \alpha n_I & -\alpha \left(\frac{\beta}{\beta+1} n_I - 1 \right) & -\alpha \frac{1}{\beta+1} n_I \\ \alpha n_I & -\alpha \frac{\beta}{\beta+1} n_I & -\alpha \left(\frac{1}{\beta+1} n_I - 1 \right) \end{bmatrix} \begin{bmatrix} \tanh(g x_E) \\ \tanh(g x_{I_1}) \\ \tanh(g x_{I_2}) \end{bmatrix}, \quad (4.6)$$

where x_E is the activity of the synchronized excitatory cells, x_{I_1} and x_{I_2} are the activities of the two synchronized inhibitory clusters, and we used $n_E = \alpha n_I$. For any solution $(x_E, x_{I_1}, x_{I_2})^T$ to [\(4.6\)](#), $\mathbf{x} = (x_E, x_{I_1}, \dots, x_{I_1}, x_{I_2}, \dots, x_{I_2})^T$ is an equilibrium solution to [\(3.2\)](#), where x_{I_1} and x_{I_2} are repeated n_{I_1} and n_{I_2} times, respectively. We note that any solution (x_E, x_{I_1}, x_{I_2}) to [\(4.6\)](#) is bounded for all g , since the matrix in [\(4.6\)](#) is constant, and $|\tanh y| \leq 1$ for all y .

The simplest case occurs when n_I is even and $\beta = 1$, in which case $n_{I_1} = n_{I_2}$. On this branch, $x_E = 0$, and $x_{I_2} = -x_{I_1}$, i.e. there are two equally sized inhibitory populations with equal and opposite activities, and there is no excitatory cell activity. Beginning with the single remaining equation for x_{I_1} , and utilizing the Taylor expansion for the tanh function, we show (see detailed calculations in [Appendix A](#)) that the nonzero solution for x_I is given, to leading order, by

$$x_I = \sqrt{\frac{3(g - g_0)}{g^3}} \quad g \geq g_0. \quad (4.7)$$

By keeping up to fifth-order terms in the Taylor expansion (see detailed calculations in [Appendix A](#)), we can obtain the higher order approximation

$$x_I = \frac{1}{2} \sqrt{\frac{5}{g^2} - \frac{\sqrt{5}g^5(24g_0 - 19g)}{g^5}} \quad g \geq g_0. \quad (4.8)$$

Comparison between the third-order approximation [\(4.7\)](#), the fifth-order approximation [\(4.8\)](#), and the numerical solution obtained by parameter continuation is shown in the left panel of [Figure 4.1](#).

For $\beta > 1$, it is no longer true that $x_{I_2} = -x_{I_1}$. However, by making an appropriate ansatz and proceeding as described in [Appendix A](#), we obtain the following approximations for x_E , x_{I_1} , and x_{I_2} in terms of g , for g close to g_0

$$x_E = \mathcal{O}\left(\frac{1}{N^2}\right), \quad x_{I_1} = \sqrt{\frac{3(g - g_0)}{(1 - \beta + \beta^2)g^3}} + \mathcal{O}\left(\frac{1}{N^2}\right), \quad x_{I_2} = -\beta x_{I_1} + \mathcal{O}\left(\frac{1}{N^2}\right) \quad g \geq g_0. \quad (4.9)$$

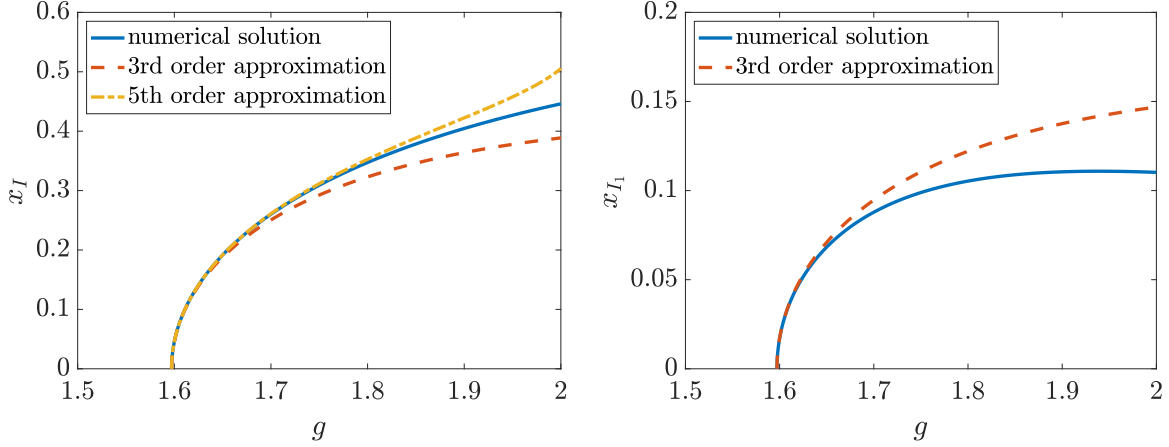


Figure 4.1. Approximations to the location of x_I on I_1/I_2 fixed point branches. Left: Third order (4.7) and fifth order (4.8) approximations to $x_I = x_{I_1}$ on the $\beta = 1$ (i.e. $n_{I_1} = n_{I_2}$) branch. Right: Third order approximation (4.9) to x_{I_1} on the $\beta = 3$ branch. Other parameters are: $N = 20$, $\alpha = 4$, $\mu_{EE} = 0.7$.

Note that this reduces to (4.7) when $\beta = 1$. In addition, we note that x_{I_1} and x_{I_2} have opposite signs. This is, in fact, true for all $g > g_0$, as shown in Appendix A. Comparison between this approximation and the numerical solution obtained by numerical parameter continuation is shown in the right panel of Figure 4.1.

4.4. Stability and bifurcations along I_1/I_2 branches. Now that we have obtained a leading order formula for the fixed points on the I_1/I_2 branches for all valid inhibitory cell ratios β , we will analyze their stability for g close to the bifurcation point g_0 . Choose any $\beta \geq 1$, so that $n_{I_1} = \frac{\beta}{\beta+1}n_I$ and $n_{I_2} = \frac{1}{\beta+1}n_I$, and let $\mathbf{x} = (x_E, x_{I_1}, x_{I_2})$ be a solution to (4.6) for $g > g_0$. To examine the stability and bifurcations which occur along the I_1/I_2 branches, we look at the linearization $D\tilde{F}(\mathbf{x}^*)$, which is given by (3.5), where $\mathbf{x}^* = (x_E, x_{I_1}, \dots, x_{I_1}, x_{I_2}, \dots, x_{I_2})^T$, and x_{I_1} and x_{I_2} are repeated n_{I_1} and n_{I_2} times, respectively. As discussed above in section 3, stability will depend on the eigenvalues of $\tilde{H}(\mathbf{x}^*)$. A cartoon showing the location of these eigenvalues is given in Figure 4.3. In the process of our analysis, we will show that a Hopf bifurcation occurs along each I_1/I_2 branch, and will find a leading order formula for its location.

To locate the eigenvalues of $\tilde{H}(\mathbf{x}^*)$, we first linearize the three-dimensional system (4.6) about the fixed point $\mathbf{x} = (x_E, x_{I_1}, x_{I_2})$ to get the Jacobian

$$J_3(\mathbf{x}) = \frac{g}{\sqrt{N}}H_3(\mathbf{x}) - I_3 \quad (4.10)$$

where

$$H_3(\mathbf{x}) = \mu_{EE} \begin{bmatrix} (\alpha n_I - 1) \operatorname{sech}^2(gx_E) & -\alpha \frac{\beta}{\beta+1} n_I \operatorname{sech}^2(gx_{I_1}) & -\alpha \frac{1}{\beta+1} n_I \operatorname{sech}^2(gx_{I_2}) \\ \alpha n_I \operatorname{sech}^2(gx_E) & -\alpha \left(\frac{\beta}{\beta+1} n_I - 1 \right) \operatorname{sech}^2(gx_{I_1}) & -\alpha \frac{1}{\beta+1} n_I \operatorname{sech}^2(gx_{I_2}) \\ \alpha n_I \operatorname{sech}^2(gx_E) & -\alpha \frac{\beta}{\beta+1} n_I \operatorname{sech}^2(gx_{I_1}) & -\alpha \left(\frac{1}{\beta+1} n_I - 1 \right) \operatorname{sech}^2(gx_{I_2}) \end{bmatrix} \quad (4.11)$$

and I_3 is the 3×3 identity matrix. We have the following proposition relating the eigenvalues of $H_3(\mathbf{x})$ and $\tilde{H}(\mathbf{x}^*)$.

Proposition 4.2. Let $\mathbf{x} = (x_E, x_{I_1}, x_{I_2})$ be a solution of (4.6) and \mathbf{x}^* the corresponding fixed point of (3.3), and let $H_3(\mathbf{x})$ and $\tilde{H}(\mathbf{x}^*)$ be defined by (4.11) and (3.6). Then

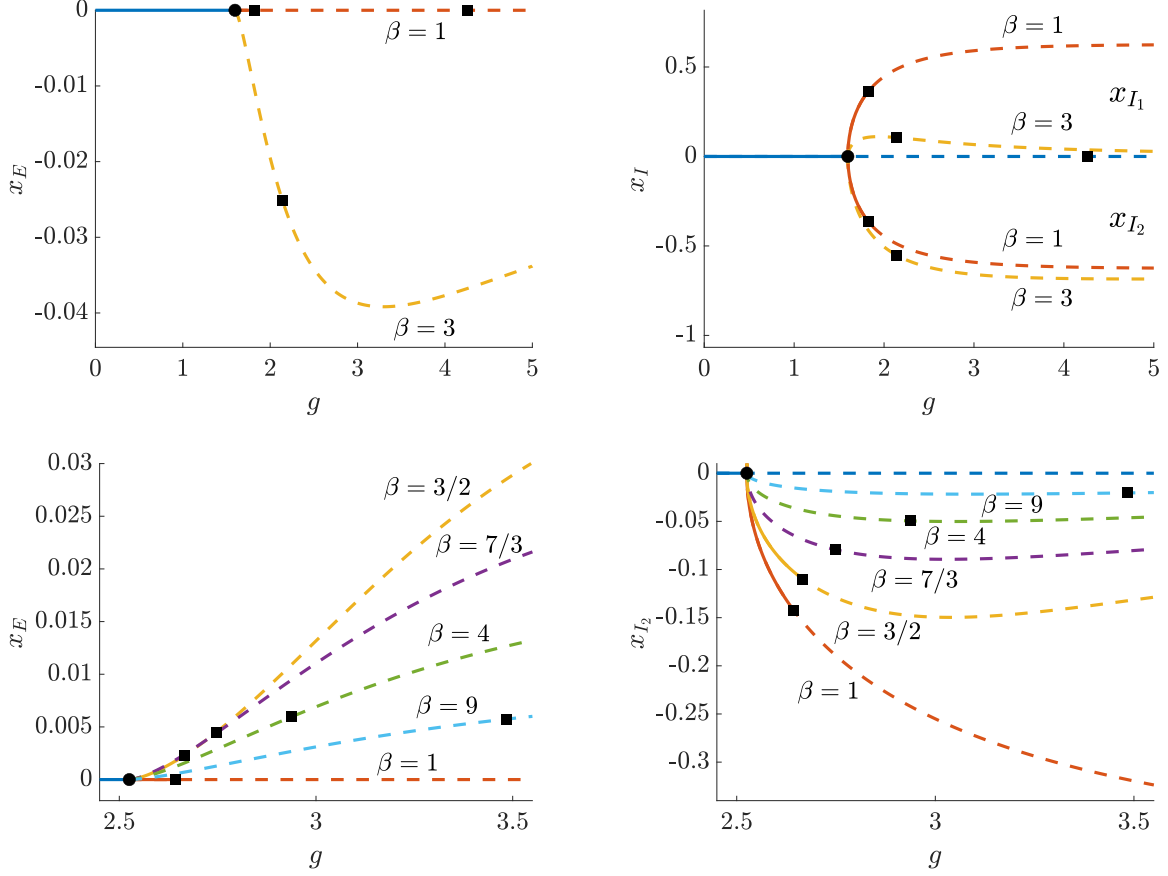


Figure 4.2. Bifurcation diagram of all possible I_1/I_2 branches of equilibria for small N networks. Top row: $N = 20$. Top left: x_E vs g . Top right: x_{I_1} (above horizontal axis) and x_{I_2} (below horizontal axis) vs g . Bottom row: $N = 50$. Bottom left: x_E vs g . Bottom right: x_{I_2} only vs g . Line format indicates stable (solid) vs. unstable (dashed) fixed points. The symmetric pitchfork bifurcation at $g = g_0$ is indicated with a filled circle. Hopf bifurcations are indicated with filled squares. Further bifurcations along branches are not shown to avoid clutter. Other parameters are $\alpha = 4$, $\mu_{EE} = 0.7$.

- (i) Every eigenvalue of $H_3(\mathbf{x})$ is an eigenvalue of $\tilde{H}(\mathbf{x}^*)$.
(ii) $\tilde{H}(\mathbf{x}^*)$ has the following additional eigenvalues:
- $\lambda_{I_1} := \mu_{EE}\alpha \operatorname{sech}^2(gx_{I_1})$ with multiplicity $n_{I_1} - 1$.
 - $\lambda_{I_2} := \mu_{EE}\alpha \operatorname{sech}^2(gx_{I_2})$ with multiplicity $n_{I_2} - 1$

Proof. For part (i), if λ is an eigenvalue of $H_3(\mathbf{x})$ with eigenvector $\mathbf{v} = (v_E, v_{I_1}, v_{I_2})$, then λ is also an eigenvalue of $\tilde{H}(\mathbf{x}^*)$ with eigenvector $\mathbf{v} = (v_E, v_{I_1}, \dots, v_{I_1}, v_{I_2}, \dots, v_{I_2})$, where v_{I_1} and v_{I_2} are repeated n_{I_1} and n_{I_2} times. For part (ii), if $n_{I_1} > 1$, then it can be verified directly that $\tilde{H}(\mathbf{x}^*)$ has an eigenvalue $\lambda_{I_1} = \mu_{EE}\alpha \operatorname{sech}^2(gx_{I_1})$ with multiplicity $n_{I_1} - 1$. The corresponding eigenvectors are $\mathbf{v}^1, \dots, \mathbf{v}^{n_{I_1}-1}$, where $v_2^k = -1$, $v_{k+2}^k = 1$, and all other components are 0. If $n_{I_2} > 1$, the eigenvalue λ_{I_2} can be similarly obtained. ■

We note that the eigenvalues λ_{I_1} and λ_{I_2} split off from λ_I at the pitchfork bifurcation point $g = g_0$; if $\mathbf{x}^* = 0$, then $\lambda_{I_1} = \lambda_{I_2} = \lambda_I$. To determine the stability of \mathbf{x}^* for g close to g_0 , we must compute the eigenvalues $\lambda_{I_1}^*(g)$ and $\lambda_{I_2}^*(g)$ of $D\tilde{F}(\mathbf{x}^*)$ corresponding to λ_{I_1} and λ_{I_2} . We will find (see Appendix B) that $\lambda_{I_2}^*(g)$ is always negative, while $\lambda_{I_1}^*(g)$ is negative for $\beta < 2$ and positive otherwise. Therefore the fixed point is unstable for $\beta \geq 2$ (see Figure 4.2).

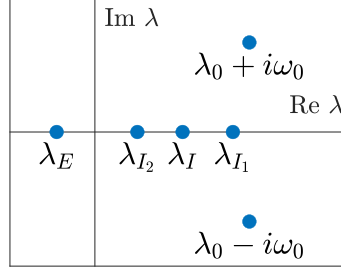


Figure 4.3. Eigenvalue pattern of the connectivity matrix $H(\mathbf{x}^*)$ for fixed point \mathbf{x}^* on I_1/I_2 branch with $\beta > 1$. The notation for the eigenvalues is explained in [subsection 4.4](#).

The remaining eigenvalues of $D\tilde{F}(\mathbf{x}^*)$ are the eigenvalues of $J_3(\mathbf{x})$, given by [\(4.10\)](#). These include one real eigenvalue and a complex pair (see [Appendix B](#) for computations). The real eigenvalue is always negative, and the complex pair crosses the real axis at a Hopf bifurcation when $g = g_H(\beta)$, where

$$g_H(\beta) = \frac{\sqrt{N}}{\mu_{EE}} \frac{2 - 5\beta + 2\beta^2 + 3\beta n_I}{\alpha(1 - 4\beta + \beta^2) - (1 - \beta + \beta^2) + 3\alpha\beta n_I} + \mathcal{O}\left(\frac{1}{N^{3/2}}\right). \quad (4.12)$$

A plot of $g_H(\beta)$ versus N for various β is given in [Figure 4.4](#). We note that a Hopf bifurcation for a particular value of β will only occur in a real network if the ratio of inhibitory cells is valid for that particular value of N (e.g. for $\beta = 3$, the total number of inhibitory cells must be a multiple of 4). The leading order term of [\(4.12\)](#), as well as the order of the remainder term, agrees with results from numerical parameter continuation ([Figure 4.4](#)). As $N \rightarrow \infty$, which implies $n_I = fN \rightarrow \infty$, the first terms in the numerator and denominator of [\(4.12\)](#) dominate, thus $g_H(\beta) \rightarrow g_0$ as $N \rightarrow \infty$ for all β (see [Figure 4.4](#)). Differentiating the leading order term in [\(4.12\)](#) with respect to β and simplifying,

$$\frac{\partial}{\partial \beta} g_H(\beta) = \frac{\sqrt{N}}{\mu_{EE}} \frac{3(\alpha + 1)(\beta^2 - 1)(n_I - 1)}{[\alpha(1 - 4\beta + \beta^2) - (1 - \beta + \beta^2) + 3\alpha\beta n_I]^2}, \quad (4.13)$$

which is 0 at $\beta = 1$ and positive for $\beta > 1$. As a consequence, $g_H(\beta)$ increases with β for $\beta \geq 1$ (see [Figure 4.4](#) for this ordering in β , as well as [Figure 4.2](#)).

4.5. Periodic solutions. Limit cycles arise as the bifurcation parameter g passes through each Hopf bifurcation point. First, we discuss the limit cycle which bifurcates from the origin at $g = g_H$. Numerical computation with AUTO [\[14\]](#) suggests that this limit cycle exists for all $g > g_H$, and that all excitatory cells are synchronized and all inhibitory cells are synchronized within this limit cycle. Since $n_{I_1} = n_I$ and $n_{I_2} = 0$, we will call this the $\beta = \infty$ limit cycle. The $\beta = \infty$ limit cycle is a periodic solution to the two-dimensional system

$$\begin{aligned} \dot{x}_1 &= f_1(x_1, x_2) := -x_1 + \frac{\mu_{EE}}{\sqrt{N}} ((n_E - 1) \tanh(gx_1) - \alpha n_I \tanh(gx_2)) \\ \dot{x}_2 &= f_2(x_1, x_2) := -x_2 + \frac{\mu_{EE}}{\sqrt{N}} (n_E \tanh(gx_1) - \alpha(n_I - 1) \tanh(gx_2)), \end{aligned} \quad (4.14)$$

where x_1 represents the synchronized excitatory cell activity and x_2 represents the synchronized inhibitory cell activity. In this two-dimensional system, the origin loses stability in a Hopf bifurcation at $g = g_H$ (see [Appendix C](#) for details). We note that equation [\(4.14\)](#) is qualitatively

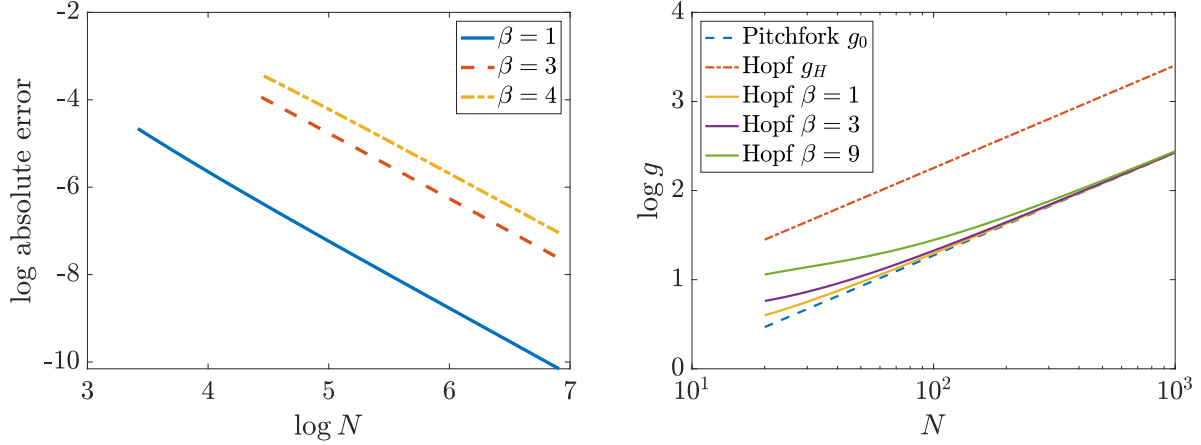


Figure 4.4. Locations of important bifurcations as a function of N . Left: Log-log plot of the absolute error of (4.12) vs N for $\beta = 1, 3$, and 4 . The slope of each line is approximately -1.5 , validating the error term $\mathcal{O}(N^{-3/2})$. Right: location of the symmetric pitchfork bifurcation g_0 (dashed line), Hopf bifurcation at the origin g_H (dash-dotted line), and Hopf bifurcations on I_1/I_2 branches (4.12) for select β (solid lines, arranged from bottom to top in order of increasing β) as a function of N . Other parameters are: $\alpha = 4$, $\mu_{EE} = 0.7$.

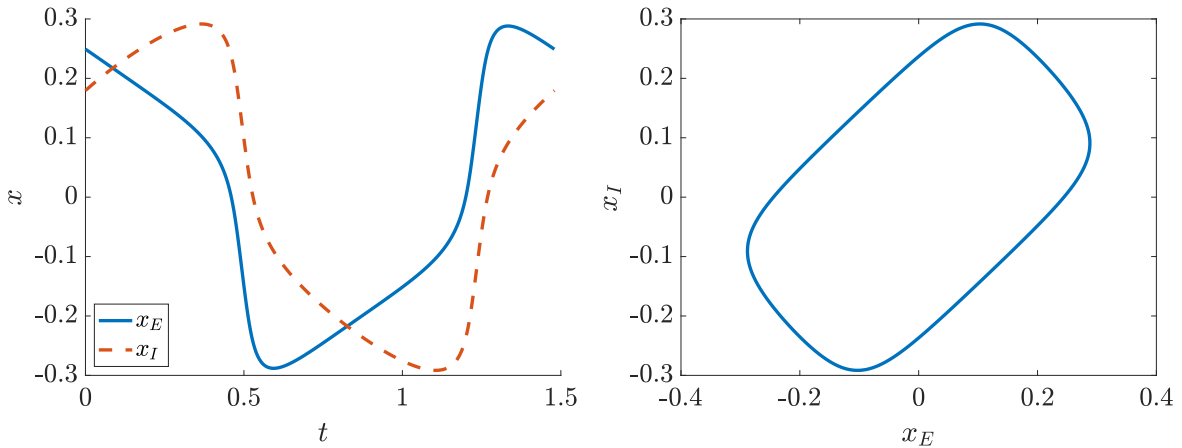


Figure 4.5. The $\beta = \infty$ limit cycle arising from a Hopf bifurcation at $g = g_H$. There is a single excitatory cluster with activity $x_E(t)$ and a single inhibitory cluster with activity $x_I(t)$. Parameters are: $N = 20$, $g = 15$, $\alpha = 4$, $\mu_{EE} = 0.7$. The period of the limit cycle is 1.62.

similar to the Wilson-Cowan model for an excitatory-inhibitory pair (see section 11.3.3 of [17]) in its “short-term memory” (STM) formulation [9]; both equations exhibit Hopf bifurcations and limit cycle solutions. The key difference is the use of input currents as bifurcation parameters in the Wilson-Cowan model as opposed to global coupling strength.

In the following proposition, we prove that the $\beta = \infty$ limit cycle exists for $g > g_H$. The proof uses the Poincaré-Bendixson theorem, and is deferred to [Appendix C](#). We note that the proposition does not address stability of the limit cycle.

Proposition 4.3. For $g > g_H$, the system (2.1) has a limit cycle in which all excitatory cells are synchronized, and inhibitory cells are synchronized. $m, m, knm/$

In addition to the $\beta = \infty$ limit cycle, periodic orbits arise at the Hopf bifurcations on each

I_1/I_2 branch as g increases through the bifurcation point. For a given I_1/I_2 branch, the associated periodic orbit has the same symmetry as that branch, i.e. all excitatory cells are synchronized, and the inhibitory cells are divided into two clusters of size n_{I_1} and n_{I_2} . For that reason, we can classify these periodic orbits in terms of the ratio $\beta = n_{I_1}/n_{I_2}$. A plot of the period of these limit cycles with increasing g is shown in [Figure 4.6](#) for $N = 20$ (see also [4, Fig. 2]) and [Figure 4.7](#) for $N = 50$. There is a critical value $g = g^*$ where all of the limit cycle branches meet (see dark band in bottom panel of [Figure 4.6](#)). For $g > g^*$, the only remaining limit cycle is the $\beta = \infty$ limit cycle, which has become stable. The point $g = g^*$ is a symmetric pitchfork bifurcation of limit cycles, which we can see by examining the Floquet multipliers of the linearization about the $\beta = \infty$ limit cycle branch (see right panel of [Figure 4.6](#)). These Floquet multipliers are computed using AUTO, and are all real. In addition to a single Floquet multiplier at 1 which is always present, there is a Floquet multiplier ρ_E with multiplicity $n_E - 1$, a Floquet multiplier ρ_I with multiplicity $n_I - 1$, and Floquet multiplier ρ_1 with multiplicity 1. At $g = g^*$, the Floquet multiplier ρ_I with multiplicity $n_I - 1$ passes through 1. As g decreases through g^* , the $\beta = \infty$ limit cycle loses stability and gives rise to limit cycles with symmetry corresponding to each I_1/I_2 branch. This is analogous to the pitchfork bifurcation of the fixed point $\mathbf{x} = 0$ at $g = g_0$, which loses stability when the eigenvalue λ_I with multiplicity $n_I - 1$ passes through the origin.

4.6. Behavior of the I_1/I_2 branch for large g . We have characterized the three-cluster fixed point solutions on the I_1/I_2 branches near the symmetric pitchfork bifurcation point at $g = g_0$. Next, we will show that these branches are unstable for sufficiently large g . Fix $\beta = n_{I_1}/n_{I_2}$, and let $\mathbf{x} = (x_E, x_{I_1}, x_{I_2})$ be a solution to (4.6) for $g > g_0$; this solution depends on g . Recall from [subsection 4.3](#) that \mathbf{x} is bounded for all g . Let \mathbf{x}^* be the corresponding fixed point of (3.3). To determine stability of \mathbf{x}^* , we will look at the eigenvalues of $D\tilde{F}(\mathbf{x}^*)$ for large g . The sum of these eigenvalues is

$$\text{Trace } D\tilde{F}(\mathbf{x}^*) = \frac{(n_E - 1)\mu_{EE}}{\sqrt{N}} g \text{sech}^2(gx_E) - (n_I + 1).$$

We will show that for sufficiently large g , $\text{Trace } D\tilde{F}(\mathbf{x}^*) > 0$, and thus at least one eigenvalue has positive real part. To do this, we analyze the behavior of x_E and $\text{sech}(gx_E)$ as $g \rightarrow \infty$. First, we consider the case when $x_E \rightarrow 0$. There are three possibilities for the behavior of $\text{sech}(gx_E)$, only two of which can occur.

- (i) $x_E \rightarrow 0$, and $gx_E \rightarrow 0$ (e.g. $x \sim g^{-\beta}$, for $\beta > 1$): then $\text{sech}^2(gx_E) \rightarrow 1$, and so $g \text{sech}^2(gx_E) \rightarrow \infty$.
- (ii) $x_E \rightarrow 0$, but $gx_E \rightarrow C$, for $C > 0$ (e.g. $x \sim g^{-1}$): then $g \text{sech}^2(gx_E) \sim g \text{sech}^2(C) \rightarrow \infty$.
- (iii) $x_E \rightarrow 0$, but $gx_E \rightarrow \infty$ (e.g. $x \sim g^{-\beta}$, for $0 < \beta < 1$). If $x_E \sim g^{-\beta}$, then $g \text{sech}^2(gx_E) \rightarrow 0$; this would seem to result in a negative trace as $g \rightarrow \infty$. However, we will show this cannot happen. Because $\text{sech}^2(gx_E) \rightarrow 0$, it follows that $\tanh^2(gx_E) \rightarrow 1$, which implies $\tanh(gx_E) \rightarrow 1$. We use the first line from (4.6) to obtain a lower bound for x_E as follows. Since x_{I_1} and x_{I_2} have opposite signs for $g > g_0$ (see the end of [Appendix A](#)), we can state that $\tanh(gx_{I_1}) \leq 1$ and $\tanh(gx_{I_2}) \leq 0$, and therefore that

$$\begin{aligned} x_E &= \frac{\mu_{EE}}{\sqrt{N}} \left[(\alpha n_1 - 1) \tanh(gx_E) - \alpha \frac{\beta}{\beta + 1} n_I \tanh(gx_{I_1}) - \alpha \frac{1}{\beta + 1} n_I \tanh(gx_{I_2}) \right] \\ &\geq \frac{\mu_{EE}}{\sqrt{N}} \left[(\alpha n_1 - 1) - \alpha \frac{\beta}{\beta + 1} n_I \right] = \frac{\mu_{EE}}{\sqrt{N}} [\alpha(n_I - n_{I_1}) - 1] \geq \frac{\mu_{EE}}{\sqrt{N}} (\alpha - 1), \end{aligned}$$

since $n_{I_1} \leq n_I - 1$. As long as we take $\alpha > 1$ (which is typically the case), x_E is bounded away from 0 for all $g > g_0$, thus contradicting our original assumption that $x_E \rightarrow 0$.

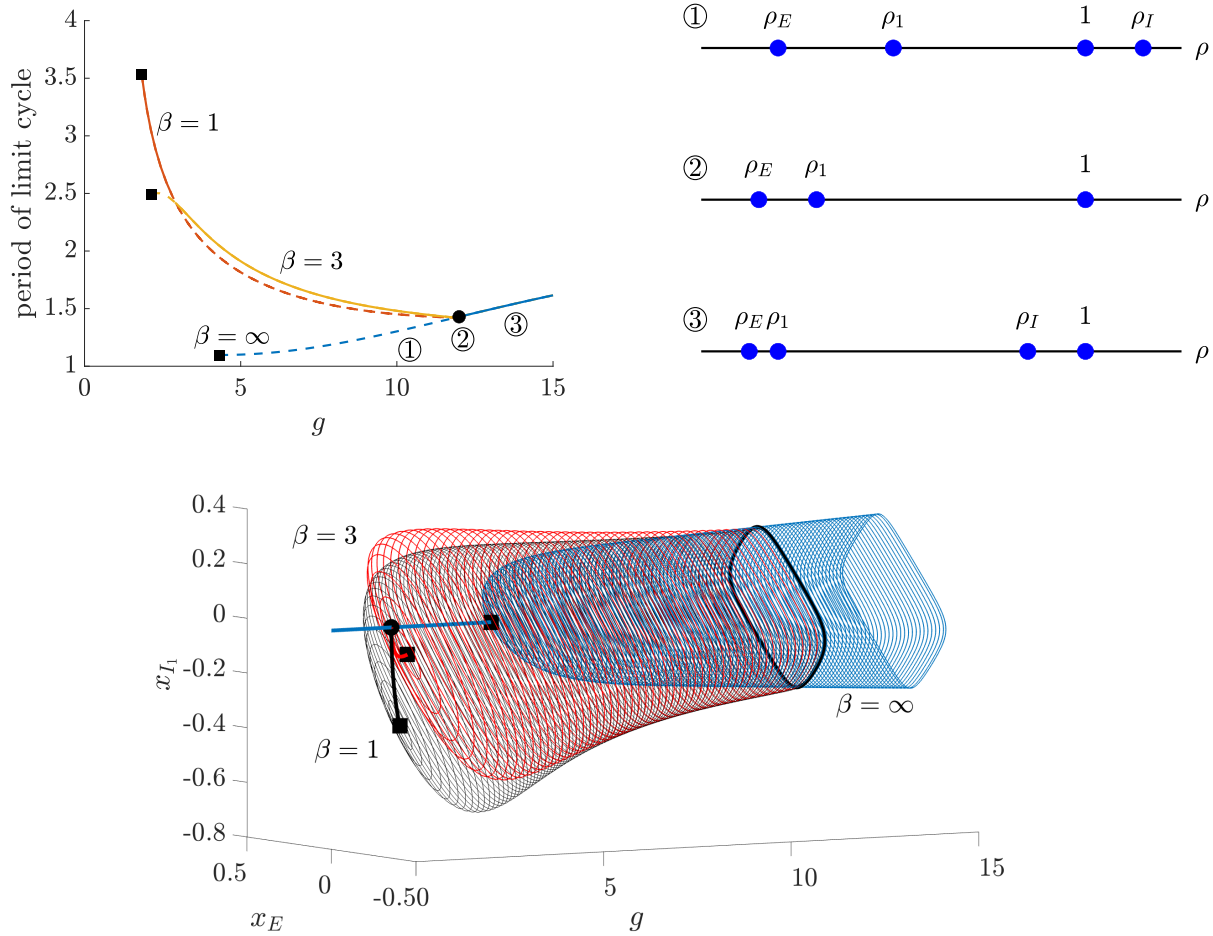


Figure 4.6. Each I_1/I_2 Hopf bifurcation spawns a branch of limit cycles which connects to the $\beta = \infty$ cycle at $g = g^*$. Top left: period of the limit cycle versus g . Stable limit cycles are indicated with solid lines. The symmetric pitchfork of limit cycles is indicated with a filled circle. Hopf bifurcations are indicated with filled squares, which correspond to the Hopf bifurcation points in Figure 4.2. Top right: Schematic of the Floquet eigenvalue pattern along the $\beta = \infty$ branch. The numbers 1, 2, and 3 identify three representative points along the $\beta = \infty$ curve in the top left panel. Bottom: (x_E, x_{I1}) vs. g for three branches of fixed points (thick lines) and limit cycles (thin lines): $\beta = 1$ (gray), $\beta = 3$ (red), and $\beta = \infty$ (blue). Other symbols are: pitchfork bifurcation at g_0 (filled circle), Hopf bifurcations for $\beta = 1$, $\beta = 3$, and $\beta = \infty$ (filled squares), and pitchfork bifurcation of limit cycles (dark band) at $g = g^*$. Parameters are: $N = 20$, $\alpha = 4$, $\mu_{EE} = 0.7$.

We have shown that if $x_E \rightarrow 0$, $\text{Trace } D\tilde{F}(\mathbf{x}^*) > 0$ for sufficiently large g , which implies that $D\tilde{F}(\mathbf{x}^*)$ always has an eigenvalue with positive real part.

The remaining possibility is that $x_E \rightarrow \hat{x}_E \neq 0$. In Appendix D, we show that this cannot occur. Therefore, all (x_E, x_{I1}, x_{I2}) satisfy $x_E \rightarrow 0$ as $g \rightarrow \infty$, and so all equilibria on the I_1/I_2 branches are unstable for sufficiently large g . We note that this does not say anything about the stability of equilibria on any branches which may bifurcate from the I_1/I_2 branches. However, the results of extensive numerical timestepping simulations suggest that there are no stable equilibria for sufficiently large g .

5. Excitatory clusters, weight parameters balanced. We now allow the excitatory cells to be grouped into n_C clusters of size p , where $p = \lfloor Nf/n_C \rfloor$. We will take $p > 1$ to ensure that each excitatory cluster contains more than one cell, and we will also assume $n_C \geq \alpha$ (e.g. $n_C \geq 4$ for

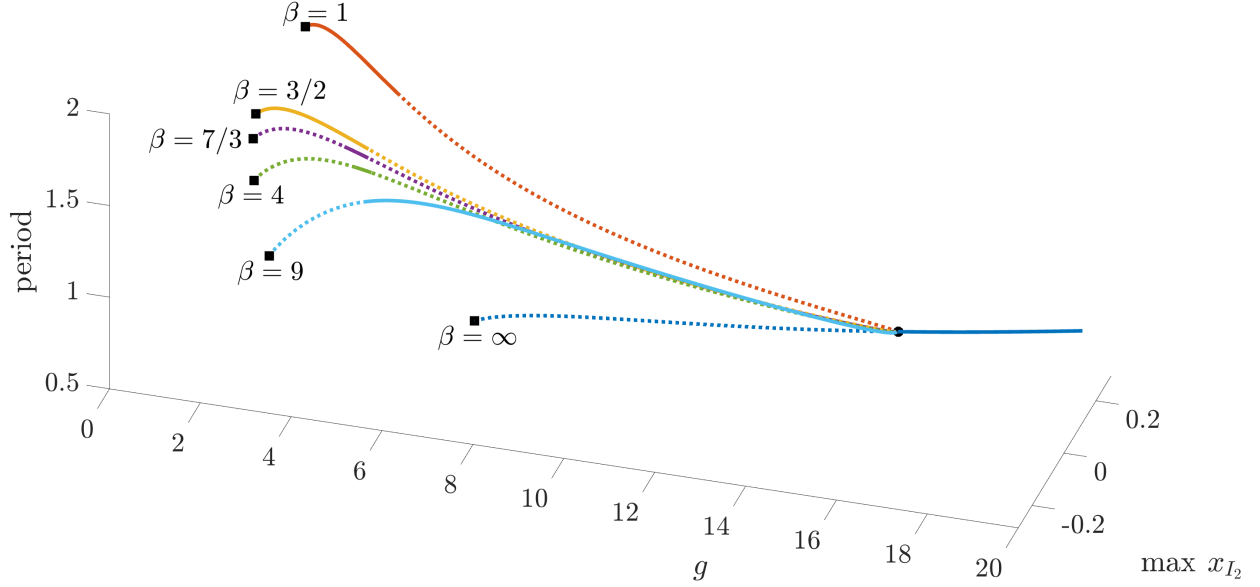


Figure 4.7. Period of limit cycle and $\max x_{I_2}$ versus g for periodic solutions arising from Hopf bifurcations. Stable limit cycles are indicated with solid lines. The symmetric pitchfork of limit cycles is indicated with a filled circle. Hopf bifurcations are indicated with filled squares. Parameters are: $N = 50$, $\alpha = 4$, $\mu_{EE} = 0.7$.

the standard value of $\alpha = 4$). Since we are interested in the behavior of the system for large N and for a large number of clusters (e.g. n_C scales with \sqrt{N}), this is not a significant restriction. Cells will be connected within, but not between, clusters. The matrix H is now

$$H = \frac{1}{\sqrt{N}} \left[\begin{array}{cccc|cc} \mu_{EE}\mathbf{K}_p & 0 & \dots & 0 & & \\ 0 & \mu_{EE}\mathbf{K}_p & \dots & 0 & & \mu_{EI}\mathbf{1}_{n_E \times n_I} \\ \vdots & \vdots & \ddots & 0 & & \\ 0 & 0 & \dots & \mu_{EE}\mathbf{K}_p & & \\ \hline & & & & \mu_{IE}\mathbf{1}_{n_I \times n_E} & \mu_{II}\mathbf{K}_{n_I} \end{array} \right] \quad (5.1)$$

which is associated with the symmetry group

$$\Gamma = \underbrace{S_p \oplus \dots \oplus S_p}_{n_C} \oplus S_{n_I} \quad p = fN/n_C.$$

As in the previous section, we choose the weights so that the network is balanced.

$$\begin{aligned} \mu_{EE} &= n_C \mu & \mu_{IE} &= \mu \\ \mu_{EI} &= -\alpha \mu & \mu_{II} &= -\alpha. \end{aligned}$$

The expression for μ_{EE} compensates for the fact that each excitatory cell has fewer excitatory connections. The eigenvalues of H (middle panel of Figure 2.1) are:

- $\lambda_I := \alpha\mu > 0$ with multiplicity $n_I - 1$
- $\lambda_E := -n_C\mu < 0$ with multiplicity $(p - 1) \times n_C = n_E - n_C$.
- $\lambda_C := (p - 1)n_C\mu > 0$, with multiplicity $n_C - 1$.
- A complex conjugate pair of eigenvalues $\lambda_0 \pm i\omega_0$, with

$$\lambda_0 := \frac{1}{2}\mu(\alpha - n_C), \quad \omega_0 := \frac{1}{2}\mu\sqrt{\alpha + n_C}\sqrt{n_C(4p - 1) - \alpha},$$

where we used the fact that $\alpha n_I = n_E = pn_C$.

Since $\lambda_E < 0$ and $\lambda_0 \leq 0$ (as a consequence of taking $n_C \geq \alpha$), the corresponding eigenvalues of $DF(0)$ will always be negative, and thus will not affect the stability of the fixed point at 0. The eigenvalues which determine stability of the origin are λ_I and λ_C . We note that since $p > 1$, $0 < \lambda_I < \lambda_C$.

As in the previous section, we will determine the bifurcations which occur as g is increased, together with the structures which emerge at these bifurcation points. First, the origin loses stability in a symmetric pitchfork bifurcation, after which point there is a branch of equilibria for every possible division of the excitatory clusters into two groups. This is similar to what occurs in the unclustered case, except the bifurcation involves the excitatory clusters instead of the inhibitory cells. As before, we derive leading order formulas for these branches, and show which of them are initially stable. As g is further increased, instead of a Hopf bifurcation, there is another symmetric pitchfork bifurcation on each of these branches, in which the inhibitory cells split into two groups. For large g , there is a collection of stable fixed points, which we can locate using the limiting behavior of the system.

5.1. Bifurcations of the origin. As the bifurcation parameter g increases from 0, the set of eigenvalues $\lambda_C^*(g)$ of $DF(0)$ corresponding to λ_C cross the imaginary axis first at

$$g = g_C := \frac{\sqrt{N}}{(p - 1)n_C\mu}. \quad (5.2)$$

When this occurs, the origin loses stability in a symmetric pitchfork bifurcation, similar to what occurs with the inhibitory cells in the previous section. As g is further increased, the eigenvalue $\lambda_I^*(g)$ crosses the imaginary axis at $g = g_0$, where g_0 is defined by (4.1). Another symmetric pitchfork bifurcation occurs at this point, this time involving the inhibitory cells. An important distinction from the previous section is that there will be no Hopf bifurcation at the origin, since the complex conjugate pair of eigenvalues cannot cross the imaginary axis.

As in the previous section, it follows from Equivariant Bifurcation Theorem that there is a branch of solutions emerging at the bifurcation point $g = g_C$ for any possible division of excitatory clusters into exactly two groups of clusters. All cells are synchronized within each excitatory cluster. Each such branch may be characterized by the number $\beta_C = n_{C_1}/n_{C_2}$, which gives the ratio of the sizes of the two groups of excitatory clusters. Without loss of generality, we may take $n_{C_1} \geq n_{C_2}$, so that $\beta_C \geq 1$. At the start of each C_1/C_2 branch, the inhibitory cells are synchronized. This is the case since, near $g = g_C$, no other eigenvalues have crossed through the origin, thus no bifurcations involving the inhibitory cells have occurred. The solution on each C_1/C_2 branch is then given as (x_{E_1}, x_{E_2}, x_I) . Due to the odd symmetry of (2.1), there is a corresponding C_1/C_2 branch for each β_C with solution $(-x_{E_1}, -x_{E_2}, -x_I)$, which we will ignore for simplicity.

5.2. Solutions on C_1/C_2 branch. First, we derive leading order expressions for the solutions along the C_1/C_2 branches for g close to g_C . The simplest case occurs when n_C is even and $\beta_C = 1$, in which case $n_{C_1} = n_{C_2}$. On this branch, $x_{E_2} = -x_{E_1}$, i.e. there are two equally sized groups of excitatory clusters with equal and opposite activity, and all the inhibitory cells have synchronized

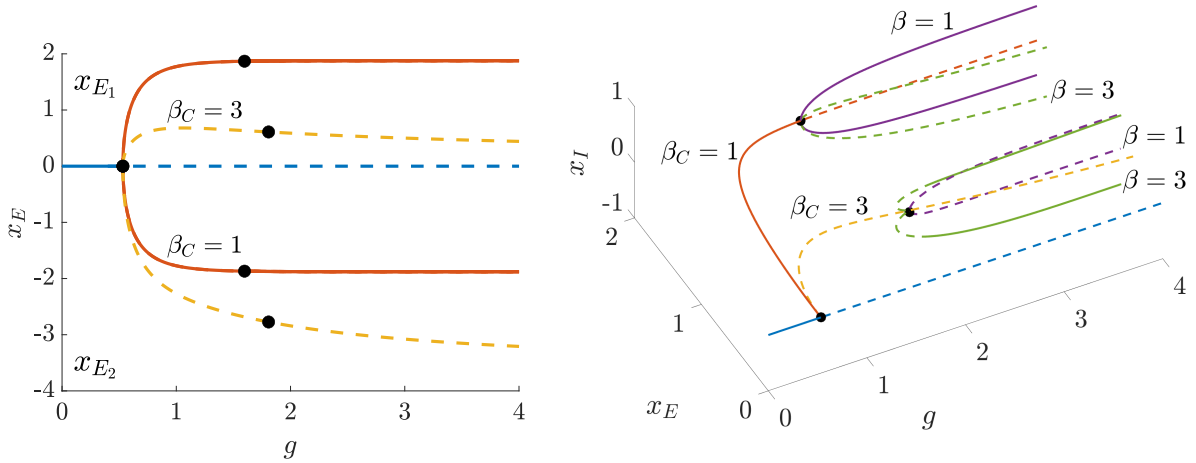


Figure 5.1. When the excitatory cells are clustered ($n_C > 1$), the first nontrivial fixed points are those for which the excitatory cells, rather than inhibitory cells, separate into two groups. Left: excitatory cell activity x_{E_1} and x_{E_2} on C_1/C_2 branches of equilibria of (2.1) with excitatory clustering for all possible values of β_C . The symmetric pitchfork bifurcations at $g = g_C$ and along the C_1/C_2 branches are indicated with filled circle. (To avoid clutter, the I_1/I_2 branches after the symmetric pitchfork bifurcation on the C_1/C_2 branch are not shown). Right: I_1/I_2 branches bifurcate from the C_1/C_2 branches (to avoid clutter only x_{E_1} is shown). Stable fixed points are indicated with solid lines. Parameters are: $N = 20$, $n_C = 4$, $p = 4$, $n_I = 4$, $\alpha = 4$, $\mu_{EE} = 0.7$.

activity $x_I = 0$. Taking $x_{E_1} = x_E$, $x_{E_2} = -x_E$, and $x_I = 0$ in (3.2) and simplifying, we obtain the single equation $\tanh(gx_E) = g_C x_E$. As in section 4, x_E is given, to leading order, by

$$x_E = \sqrt{\frac{3(g - g_C)}{g^3}} \quad g \geq g_C, \quad (5.3)$$

for g close to g_C . For $\beta_C > 1$, we find the solution along each C_1/C_2 branch by reducing (2.1) to the 3-dimensional system

$$\begin{bmatrix} x_{E_1} \\ x_{E_2} \\ x_I \end{bmatrix} = \frac{\mu}{\sqrt{N}} \begin{bmatrix} (p-1)n_C & 0 & -pn_C \\ 0 & (p-1)n_C & -pn_C \\ pn_C \frac{\beta_C}{\beta_C+1} & pn_C \frac{1}{\beta_C+1} & -(pn_C - \alpha) \end{bmatrix} \begin{bmatrix} \tanh(gx_{E_1}) \\ \tanh(gx_{E_2}) \\ \tanh(gx_I) \end{bmatrix}, \quad (5.4)$$

where we used $\alpha n_I = n_E = pn_C$. The variables x_{E_1} and x_{E_2} are the activities of the two groups of excitatory clusters, and x_I is the activity of the inhibitory cells, which are synchronized since g is close to g_C . Following the same procedure as in section 4, we obtain the following approximations for x_{E_1} , x_{E_2} , and x_I

$$x_{E_1} = \pm \sqrt{\frac{3(g - g_C)}{(1 - \beta_C + \beta_C^2)g^3}} + \mathcal{O}\left(\frac{1}{N^2}\right), \quad x_{E_2} = -\beta_C x_{E_1} + \mathcal{O}\left(\frac{1}{N^2}\right), \quad x_I = \mathcal{O}\left(\frac{1}{N^2}\right) \quad g \geq g_C, \quad (5.5)$$

for g close to g_C , which reduces to (5.3) when $\beta = 1$.

5.3. Stability and bifurcations along C_1/C_2 branch. We now analyze the stability of the C_1/C_2 branches for g close to g_C . Choose any $\beta_C \geq 1$, so that $n_{C_1} = \frac{\beta_C}{\beta_C+1}n_C$ and $n_{C_2} = \frac{1}{\beta_C+1}n_C$. Let $\mathbf{x} = (x_{E_1}, x_{E_2}, x_I)$ be a solution to (5.4). We look at the linearization $D\tilde{F}(\mathbf{x}^*)$, where

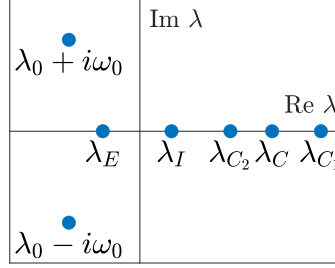


Figure 5.2. The eigenvalue pattern of the connectivity matrix $H(\mathbf{x}^*)$ for fixed points \mathbf{x}^* on a C_1/C_2 branch with $\beta_C > 1$. The notation for the eigenvalues is explained below [Proposition 5.1](#).

$\mathbf{x}^* = (x_{E_1}, \dots, x_{E_1}, x_{E_2}, \dots, x_{E_2}, x_I, \dots, x_I)^T$, where x_{E_1} and x_{E_2} are repeated n_{C_1} and n_{C_2} times, respectively, and x_I is repeated n_I times. Stability will depend on the eigenvalues of $\tilde{H}(\mathbf{x}^*)$. A cartoon showing the location of these eigenvalues is given in [Figure 5.2](#).

We follow the same procedure as in [subsection 4.4](#). First, we linearize the reduced system [\(5.4\)](#) about (x_{E_1}, x_{E_2}, x_I) to get the Jacobian

$$J_3(\mathbf{x}) = \frac{g}{\sqrt{N}} H_3(\mathbf{x}) - I_3, \quad (5.6)$$

where

$$H_3(\mathbf{x}) = \mu \begin{bmatrix} (p-1)n_C \operatorname{sech}^2(gx_{E_1}) & 0 & -pn_C \operatorname{sech}^2(gx_I) \\ 0 & (p-1)n_C \operatorname{sech}^2(gx_{E_2}) & -pn_C \operatorname{sech}^2(gx_I) \\ pn_C \frac{\beta_C}{\beta_C+1} \operatorname{sech}^2(gx_{E_1}) & pn_C \frac{1}{\beta_C+1} \operatorname{sech}^2(gx_{E_2}) & -(pn_C - \alpha) \operatorname{sech}^2(gx_I) \end{bmatrix} \quad (5.7)$$

and I_3 is the 3×3 identity matrix. We have the following proposition concerning the eigenvalues of $H_3(\mathbf{x})$ and $\tilde{H}(\mathbf{x}^*)$. The proof is omitted since it is similar to that of [Proposition 4.2](#).

Proposition 5.1. Let $\mathbf{x} = (x_{E_1}, x_{E_2}, x_I)$ be a solution to [\(5.4\)](#) and \mathbf{x}^* the corresponding fixed point of [\(3.3\)](#), and let $H_3(\mathbf{x})$ and $\tilde{H}(\mathbf{x}^*)$ be defined by [\(5.7\)](#) and [\(3.6\)](#). Then

(i) Every eigenvalue of $H_3(\mathbf{x})$ is an eigenvalue of $\tilde{H}(\mathbf{x}^*)$.

(ii) $\tilde{H}(\mathbf{x}^*)$ has the following additional eigenvalues:

- $\lambda_{C_1} := (p-1)n_C \mu \operatorname{sech}^2(gx_{E_1})$ with multiplicity $n_{C_1} - 1$.
- $\lambda_{C_2} := (p-1)n_C \mu \operatorname{sech}^2(gx_{E_2})$ with multiplicity $n_{C_2} - 1$.
- $\lambda_I := \alpha \mu \operatorname{sech}^2(gx_I)$ with multiplicity $n_I - 1$.

We note that the eigenvalues λ_{C_1} and λ_{C_2} split off from λ_C at the pitchfork bifurcation point $g = g_C$; if $\mathbf{x}^* = 0$, then $\lambda_{C_1} = \lambda_{C_2} = \lambda_C$. To determine the stability of \mathbf{x}^* for g close to g_C , we first compute the eigenvalues of $D\tilde{F}(\mathbf{x}^*)$ corresponding to λ_{C_1} , λ_{C_2} , and λ_I . We find (see [Appendix E](#)) that the cluster-associated eigenvalue $\lambda_{C_1}^*(g)$ is negative for $1 \leq \beta_C < 2$ and positive for $\beta_C > 2$; $\lambda_{C_2}^*(g)$ is negative for $\beta_C > 1/2$; and $\lambda_I^*(g)$ is negative for all β_C for N sufficiently large. The behavior of $\lambda_{C_1}^*(g)$ implies that the C_1/C_2 branches are initially unstable for $\beta_C > 2$ (see [Figure 5.1](#) and [Figure 5.4](#)).

The remaining eigenvalues of $D\tilde{F}(\mathbf{x}^*)$ are the eigenvalues of $J_3(\mathbf{x})$. Following the same procedure as in [subsection 4.4](#) (see [Appendix E](#) for details), we find that, since we are taking $n_C \geq \alpha$, the eigenvalues of $J_3(\mathbf{x})$ all have negative real part for g close to g_C . Thus the C_1/C_2 branches are initially stable for $1 \leq \beta_C \leq 2$ (see the top panel of [Figure 5.1](#) as well as [Figure 5.4](#)).

As g is further increased from g_C , there is a second symmetric pitchfork bifurcation on each C_1/C_2 branch as the eigenvalue $\lambda_I^*(g)$ of $D\tilde{F}(\mathbf{x}^*)$ crosses the origin (see bifurcation diagram in

Figure 5.1 and Figure 5.4). The behavior at this symmetric pitchfork bifurcation is much the same as in section 4: there is an I_1/I_2 branch of solutions for every possible division of the inhibitory cells into exactly two clusters. We can characterize these branches using the parameter $\beta = n_{I_1}/n_{I_2}$, as we did in the previous section. When $\beta_C = 1$, $x_I = 0$, and this bifurcation takes place at

$$g_I = \frac{\sqrt{N}}{\alpha\mu}. \quad (5.8)$$

For $\beta_C > 1$, this bifurcation takes place at g much greater than g_C , thus the approximation (5.5) no longer holds. To locate these bifurcations, we will examine the behavior of the system as g becomes large. We note here that evidence from numerical parameter continuation suggests that there are no Hopf bifurcations along the C_1/C_2 branches; furthermore, numerical timestepping experiments suggest that there are no stable periodic orbits for any value of g .

5.4. C_1/C_2 branches for large g . We look at the behavior of solutions on the C_1/C_2 branch as g becomes large. This will depend on the ratio $\beta_C = n_{C_1}/n_{C_2}$. When $\beta_C = 1$, $x_{E_2} = -x_{E_1} := x_E$, and $x_I = 0$ for all $g \geq g_C$. Numerical parameter continuation suggests that $x_E \rightarrow \hat{x}_E > 0$ as $g \rightarrow \infty$, which implies that $\tanh(gx_E) \rightarrow 1$. It follows from the first row of (5.4) that

$$\hat{x}_E = \frac{\mu}{\sqrt{N}}(p-1)n_C. \quad (5.9)$$

For $\beta_C > 1$, numerical parameter continuation suggests $x_I \rightarrow 0$ as $g \rightarrow \infty$, but $\tanh(gx_I) \rightarrow \hat{y}_I \neq 0$. There are two patterns for the limiting behavior on the C_1/C_2 branches, which depend on whether $\beta_C < \beta_C^*$ or $\beta_C > \beta_C^*$, for a critical value

$$\beta_C^* = \frac{(n_C p - \alpha)(2p - 1) + \alpha p}{n_C p + \alpha(p - 1)}. \quad (5.10)$$

(See Appendix F for a derivation of β_C^*). These are illustrated in Figure 5.3.

- Case 1: ($1 < \beta_C < \beta_C^*$) $x_{E_1} \rightarrow \hat{x}_{E_1} > 0$ and $x_{E_2} \rightarrow \hat{x}_{E_2} < 0$.
- Case 2: ($\beta_C > \beta_C^*$) $x_{E_1} \rightarrow 0$ with $\tanh(gx_{E_1}) \rightarrow \hat{y}_{E_1} \neq 0$, and $x_{E_2} \rightarrow \hat{x}_{E_2} < 0$.

As $N \rightarrow \infty$, $n_C p = fN \rightarrow \infty$ as well. If both p and n_C scale as \sqrt{N} , then the only significant terms in the numerator and denominator of (5.10) are of order N or larger, in which case $\beta_C^* \rightarrow 2p - 1$ as $N \rightarrow \infty$.

In Appendix F, we derive formulas for x_{E_1} , x_{E_2} , and x_I for both of these cases. We then use these formulas to find the location of the symmetric pitchfork bifurcation points on the C_1/C_2 branches when $\beta_C > 1$ and N is large. If we take both p and n_C to scale as \sqrt{N} , we can assume $\beta_C < \beta_C^*$, as discussed above. At this bifurcation, the eigenvalue $\lambda_I^*(g)$ of $D\tilde{F}(\mathbf{x}^*)$ with multiplicity $n_I - 1$ crosses through 0. Using the identity $\operatorname{sech}^2(gx_I) = 1 - \tanh^2(gx_I) \rightarrow 1 - \hat{y}_I^2$ as $g \rightarrow \infty$ together with (F.1), the symmetric pitchfork bifurcation on the C_1/C_2 branch is located, to leading order, at

$$g_I(\beta_C) = \frac{\sqrt{N}(1 + \beta_C)^2}{4\alpha\mu\beta_C} \quad (5.11)$$

for N large. When $\beta_C = 1$, this reduces to (5.8). See Figure 5.4 and the left panel of Figure 5.5 for the location of the symmetric pitchfork bifurcations on the C_1/C_2 branches. Numerical simulation validates this formula, and suggests that the error term in (5.11) has order $\mathcal{O}(N^{-1/2})$ (Figure 5.5, right panel). We note that for N large, $g_I(\beta_C)$ is quadratic in β_C , has a local minimum at $\beta_C = 1$,

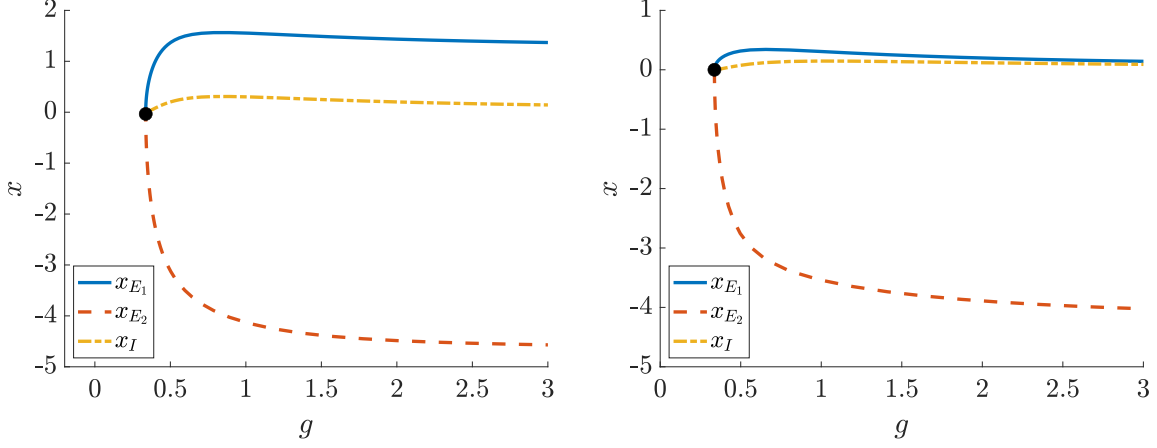


Figure 5.3. The saturation ($g \gg 1$) behavior of fixed points on a C_1/C_2 branch depends on the clustering parameter β_C . Left: x_{E_1} , x_{E_2} , and x_I vs g on C_1/C_2 branches for $1 < \beta_C < \beta_C^*$. Right: $\beta_C > \beta_C^*$. Parameters are: $N = 50$, $n_C = 10$, $p = 4$, $n_I = 10$, $\alpha = 4$, $\mu = 0.7$. Given these parameters $\beta_C^* = 5.15385$: here we illustrate $\beta_C = 7/3$ (left) and $\beta_C = 9$ (right).

and is increasing for $\beta_C > 1$. We can see in [Figure 5.4](#) and [Figure 5.5](#) that the location of the symmetric bifurcation points $g_I(\beta_C)$ increases with β_C .

For sufficiently large N , each C_1/C_2 branch will be stable immediately preceding the pitchfork bifurcation at $g_I(\beta_C)$. To see this, we evaluate the remaining eigenvalues of $D\tilde{F}(\mathbf{x}^*)$ when $g = g_I(\beta_C)$. As $N \rightarrow \infty$, $g_I(\beta_C) \rightarrow \infty$, thus $\text{sech}(g_I(\beta_C)x_{E_j}) \rightarrow 0$ for $j = 1, 2$. It follows that for $g = g_I(\beta_C)$, $\lambda_{C_j} \rightarrow 0$, thus $\lambda_{C_j}^*(g) \rightarrow -1$ for $j = 1, 2$. By the same argument, taking $N \rightarrow \infty$ will zero out the first two columns of (5.7) when $g = g_I(\beta_C)$. Thus, in the limit $N \rightarrow \infty$, $H_3(\mathbf{x}^*)$ will have a pair of eigenvalues at 0 and an additional eigenvalue at $-(pn_C - \alpha) \text{sech}^2 gx_I \leq 0$. The corresponding eigenvalues of $D\tilde{F}(\mathbf{x}^*)$ will be negative.

As an example, consider the $N = 100$ system shown in [Figure 5.4](#). The C_1/C_2 branches for $\beta_C = 7/3, 4$, and 9 start unstable, but regain stability before the symmetric pitchfork bifurcation points. This does not necessarily occur for small values of N (see [Figure 5.1](#) for $N = 20$, where this does not happen).

5.5. Stability of $C_1/C_2/I_1/I_2$ solutions for large g . After the symmetric pitchfork bifurcation point on the C_1/C_2 branches, both the excitatory clusters and inhibitory cells have split into two populations. We are interested in stable fixed points when g is large. In particular, we seek fixed point branches in which the excitatory clusters are split into two populations with ratio $\beta_C = n_{C_1}/n_{C_2}$, and the inhibitory cells are also split into two populations with ratio $\beta = n_{I_1}/n_{I_2}$. This reduces (2.1) to the system of equations

$$\begin{bmatrix} x_{E_1} \\ x_{E_2} \\ x_{I_1} \\ x_{I_2} \end{bmatrix} = \frac{\mu}{\sqrt{N}} \begin{bmatrix} (p-1)n_C & 0 & -\alpha \frac{\beta}{\beta+1} n_I & -\alpha \frac{1}{\beta+1} n_I \\ 0 & (p-1)n_C & -\alpha \frac{\beta}{\beta+1} n_I & -\alpha \frac{1}{\beta+1} n_I \\ pn_C \frac{\beta_C}{\beta_C+1} & pn_C \frac{1}{\beta_C+1} & -\alpha \left(\frac{\beta}{\beta+1} n_I - 1 \right) & -\alpha \frac{1}{\beta+1} n_I \\ pn_C \frac{\beta_C}{\beta_C+1} & pn_C \frac{1}{\beta_C+1} & -\alpha \frac{\beta}{\beta+1} n_I & -\alpha \left(\frac{1}{\beta+1} n_I - 1 \right) \end{bmatrix} \begin{bmatrix} \tanh(gx_{E_1}) \\ \tanh(gx_{E_2}) \\ \tanh(gx_{I_1}) \\ \tanh(gx_{I_2}) \end{bmatrix}. \quad (5.12)$$

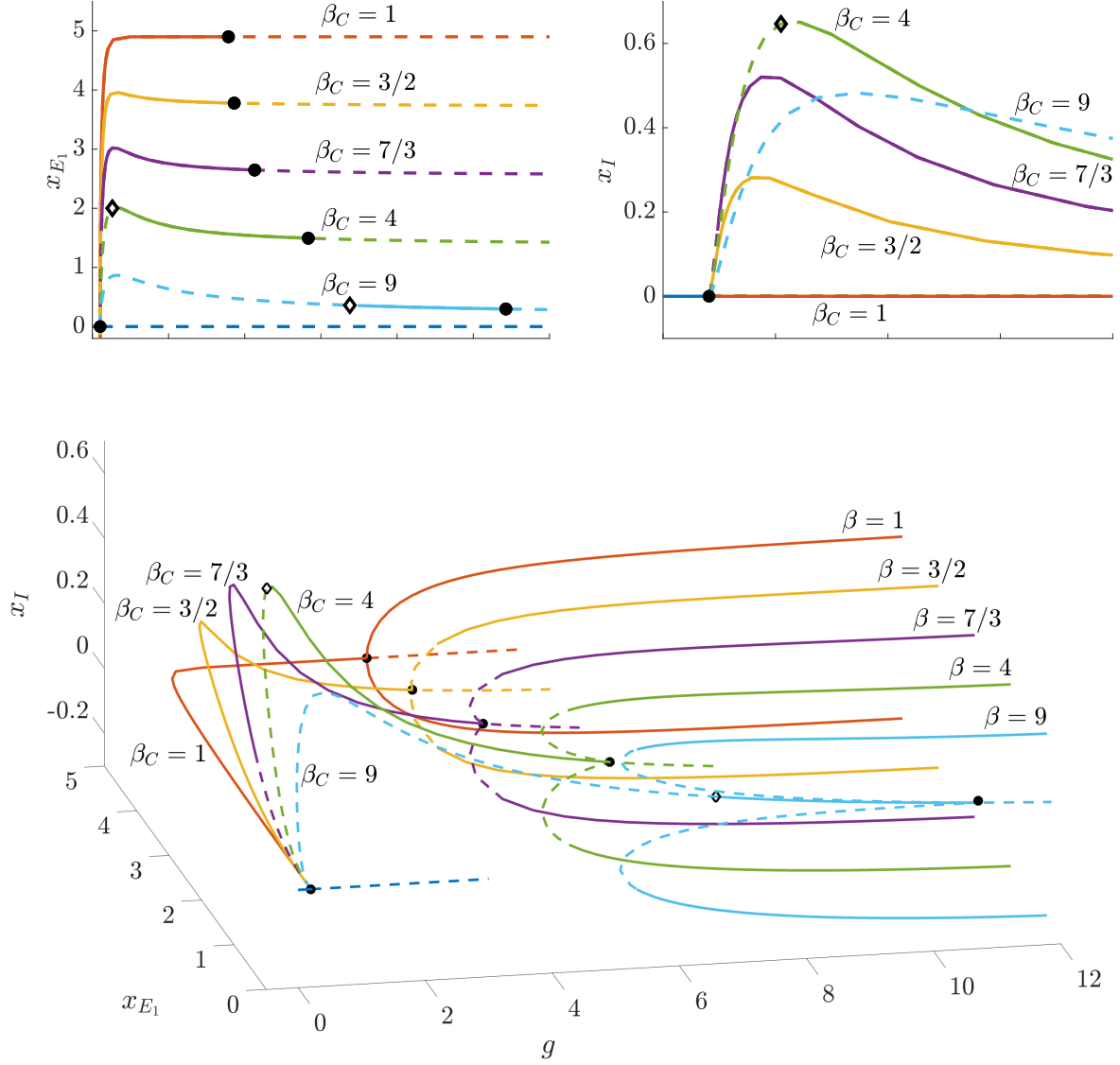


Figure 5.4. Bifurcation diagram of all possible C_1/C_2 branches, and selected $C_1/C_2/I_1/I_2$ branches, for a moderate value of N . Top: C_1/C_2 branches of equilibria of (2.1) with excitatory clustering for all possible values of β_C . Top left: x_{E_1} vs g . Top right: x_I vs g , zoomed into a narrower range of g to show stability of C_1/C_2 branches near $g = g_C$. Symmetric pitchfork bifurcations at $g = g_C$ and along the C_1/C_2 branches are indicated with filled circle. To avoid clutter, the $C_1/C_2/I_1/I_2$ branches are not shown. Bottom: x_I and x_{E_1} vs. g , for $C_1/C_2/I_1/I_2$ branches bifurcating from the C_1/C_2 branches. The only I_1/I_2 branches shown here are the ones which are eventually stable, which in this case are those with $\beta = \beta_C$ (see Table 5.1). Stable fixed points are indicated with solid lines, unstable fixed points with dashed line. Unstable C_1/C_2 branches for $\beta_C = 4$ and $\beta_C = 9$ become stable at the points indicated with the diamond. Parameters are: $N = 100$, $n_C = 10$, $p = 8$, $n_I = 20$, $\alpha = 4$, $\mu_{EE} = 0.7$.

Parameter continuation suggests that as $g \rightarrow \infty$, $(x_{E_1}, x_{E_2}, x_{I_1}, x_{I_2}) \rightarrow (\hat{x}_{E_1}, \hat{x}_{E_2}, \hat{x}_{I_1}, \hat{x}_{I_2})$, where $\hat{x}_{E_1}, \hat{x}_{I_1} > 0$ and $\hat{x}_{E_2}, \hat{x}_{I_2} < 0$. Such solutions exist for

$$\frac{2\beta n_I - \beta - 1}{2n_I + \beta + 1} < \beta_C < \frac{2\beta n_I + \beta + 1}{2n_I - \beta - 1}. \quad (5.13)$$

for all valid β satisfying $1 \leq \beta < 2p - 1$. See Appendix G for detailed calculations.

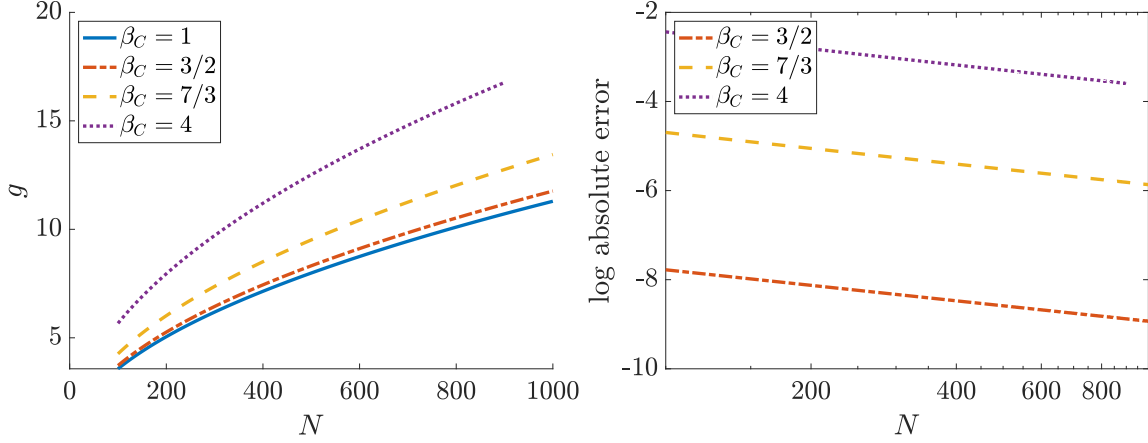


Figure 5.5. Location of the symmetric pitchfork bifurcation points on C_1/C_2 branches. Left: $g_I(\beta_C)$ vs. N for various β_C . Right: semi-log plot of the absolute error of approximation (5.11) vs N for various β_C . The slope of each line is approximately -0.5 (validating the error term $\mathcal{O}(N^{-1/2})$). Parameters are: $n_C = 10$, $\alpha = 4$, $\mu = 0.7$.

N	n_I	n_C	p	(β, β_C)
20	4	4	4	(1, 1), (3, 3)
25	5	5	4	(3/2, 3/2), (4, 4)
25	5	4	5	(4, 3)
35	7	7	4	(4/3, 4/3), (5/2, 5/2), (6, 6)
35	7	4	7	(5/2, 3)
50	10	10	4	(1, 1), (3/2, 3/2), (7/3, 7/3), (4, 4)
100	20	10	8	(1, 1), (3/2, 3/2), (7/3, 7/3), (4, 4), (9, 9)

Table 5.1

Valid pairs (β, β_C) which satisfy (5.13), for selected values of N , n_C and n_I . (Note that $\alpha = 4$ in all cases, which determines n_I and p_{n_C}).

For some small values of N , a list of all valid pairs of (β, β_C) which satisfy (5.13) is given in Table 5.1. (A value of β or β_C is valid for a particular N only if the ratio of inhibitory cells or excitatory clusters is possible for that value of N). In the specific case where $n_C = n_I$, it follows from (5.13) that

$$n_{I_1} - \frac{1}{2} < n_{C_1} < n_{I_1} + \frac{1}{2}.$$

Since n_{C_1} must be an integer, $n_{C_1} = n_{I_1}$, which implies $\beta_C = \beta$.

The fixed point \mathbf{x}^* corresponding to each of these (β, β_C) is eventually stable for sufficiently large g , since as $g \rightarrow \infty$, $H(\mathbf{x}^*)$ approaches the $\mathbf{0}$ matrix, thus the Jacobian $DF(\mathbf{x}^*)$ approaches $-I$, which has a single eigenvalue of -1 with multiplicity N . The solutions corresponding to the top row of Table 5.1 are shown in the bottom panel of Figure 5.1, and the solutions corresponding to the bottom row are shown in the bottom panel of Figure 5.4; we can see from the figures that the corresponding fixed points are all stable for sufficiently large g .

5.6. Excitatory clusters with weight parameters unchanged. We briefly consider a system with excitatory clusters, but in which we have not adjusted the excitatory weight strengths, i.e. $\mu_{EI} = -\alpha\mu_{EE}$, $\mu_{II} = -\alpha\mu_{EE}$, and $\mu_{IE} = \mu_{EE}$. In this case, the two eigenvalues of H with positive

real part are $\lambda_I = \alpha\mu_{EE}$ and $\lambda_C = (p-1)\mu_{EE}$. If $\lambda_C > \lambda_I$, which occurs when $n_C < \frac{fN}{\alpha+1}$, the behavior is qualitatively the same as for the case balanced weight parameters discussed above. If $\lambda_C < \lambda_I$, which occurs when $n_C > \frac{fN}{\alpha+1}$, the order of the two symmetric pitchfork bifurcations is reversed. As g is increased, the inhibitory cells bifurcate from the origin first, followed by the excitatory clusters.

5.7. Restored self-coupling. We can restore self-coupling of neurons with each excitatory cluster by replacing the matrix \mathbf{K}_p in (5.1) with the $p \times p$ matrix consisting of all 1s. The effect of this in the reduced model (3.3) is to replace the matrix $(p-1)\mu_{EE}I_{n_C}$ in the upper left block of (3.4) with $p\mu_{EE}I_{n_C}$. The eigenvalues of H are then given by:

- $\lambda_I := \alpha\mu > 0$ with multiplicity $n_I - 1$
- $\lambda_E := 0$ with multiplicity $(p-1) \times n_C = n_E - n_C$.
- $\lambda_C := pn_C\mu > 0$, with multiplicity $n_C - 1$.
- A complex conjugate pair of eigenvalues $\lambda_0 \pm i\omega_0$, with

$$\lambda_0 := \frac{1}{2}\mu\alpha, \quad \omega_0 := \frac{1}{2}\mu\sqrt{\alpha(4n_Cp - \alpha)},$$

The eigenvalue pattern is similar to that in the middle panel of Figure 2.1, except the complex conjugate pair $\lambda_0 \pm i\omega_0$ has positive real part. As a consequence, there will be a Hopf bifurcation at the origin at $g_H = \sqrt{N}/\alpha\mu$. Parameter continuation with AUTO indicates that the resulting limit cycle has all excitatory clusters synchronized and all inhibitory cells synchronized, and is unstable for $g > g_H$. In addition, timestepping simulations suggest that there are no stable limit cycles for any value of g . The pattern of symmetric pitchfork bifurcations, first at the origin and then on each C_1/C_2 branch, is the same as for the case with no self-coupling.

6. Inhibitory clusters. We will briefly consider the case where the inhibitory cells are clustered, while the excitatory cells remain unclustered. Suppose the inhibitory cells are grouped into n_{C_I} inhibitory clusters of size p_I . For the choice of weights $\mu_{EI} = -\alpha\mu_{EE}$, $\mu_{II} = -\alpha\mu_{EE}$, and $\mu_{IE} = \mu_{EE}$, the eigenvalues of H are:

- $\lambda_I := \alpha\mu_{EE} > 0$ with multiplicity $(p_I - 1) \times n_{C_I} = n_I - n_{C_I}$.
- $\lambda_E := -\mu_{EE} < 0$ with multiplicity $n_E - 1$.
- $\lambda_{C_I} := -(p_I - 1)\alpha\mu_{EE} < 0$, with multiplicity $n_{C_I} - 1$.
- A complex conjugate pair of eigenvalues $\lambda_0 \pm i\omega_0$, with

$$\lambda_0 := \frac{1}{2}\mu_{EE}[\alpha(1 + p_I(n_{C_I} - 1)) - 1]$$

$$\omega_0 := \sqrt{a^2 \left((-3n_{C_I}^2 + 2n_{C_I} + 1) p_I^2 - 2(n_{C_I} + 1)p_I + 1 \right) - 2a(n_{C_I}p_I + p_I - 1) + 1},$$

where we used the fact that $n_E = \alpha n_{C_I} p_I$.

The two eigenvalues with positive real part are λ_I and $\lambda_0 + i\omega_0$, so these are the only eigenvalues which will cause bifurcations as g is varied. We note that $\lambda_0 > \lambda_I$, thus the first bifurcation which will occur at the origin is a Hopf bifurcation at

$$g_H = \frac{2\sqrt{N}}{\mu_{EE}[\alpha(1 + p_I(n_{C_I} - 1)) - 1]}.$$

We are interested in what occurs for large N and large n_{C_I} . As an example, let n_{C_I} scale with \sqrt{N} by taking $n_{C_I} = p_I = \sqrt{n_I} = \sqrt{(1-f)N}$. For this scaling, as N increases, the Hopf bifurcation takes place at $g_H \approx \frac{2}{f\mu_{EE}\sqrt{N}}$, and we also have $\omega_0 \approx \frac{\sqrt{3}}{2}fN\mu_{EE}$. This implies that at $g = g_H$,

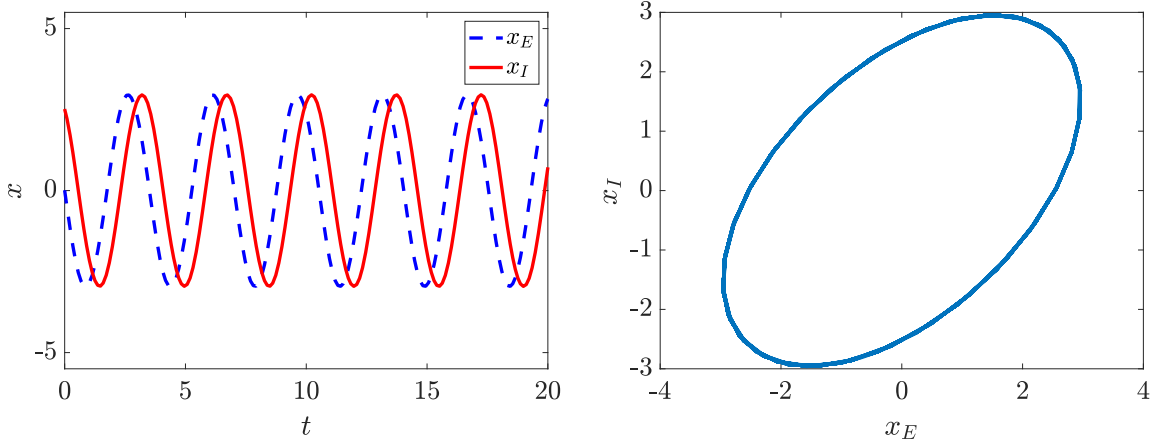


Figure 6.1. Limit cycle arising from the Hopf bifurcation at origin for (2.1) with inhibitory cell clustering and $\mu_{II} = -\alpha\mu_{EE}$. Both the excitatory cell activity x_E and inhibitory cell activity x_I are synchronized. Notably, the period does not increase with N . Left: x_E and x_I vs t . Right: x_I vs x_E . Parameters are: $N = 1600$, $N_{C_I} = 20$, $p_I = 20$, $\alpha = 4$, $\mu_{EE} = 0.7$, $g = 1.02g_H$. The period of the limit cycle is 1.792.

$DF(0)$ has a complex conjugate pair of eigenvalues with real part of 0 and imaginary part of approximately $\sqrt{3}$. See Figure 6.1 for an illustration of this limit cycle when $N = 1600$, $n_{C_I} = 20$, and g is slightly larger than g_H . The frequency of the limit cycle is 1.792, which is less than 5% away from $\sqrt{3}$. Thus, for large N , the frequency of the limit cycle emerging at the Hopf bifurcation of the origin is asymptotically constant as N increases. This contrasts to the case where the inhibitory and excitatory cells are unclustered, where the frequency of the limit cycle scales as \sqrt{N} .

7. Discussion. In this paper, we analyze a family of clustered excitatory-inhibitory neural networks, and, in particular, the underlying bifurcation structures that arise because of permutation symmetries in the network. For the simplest case, an all-to-all connected network which excludes self-connections, we extend the results in [4] to provide a more complete picture of the bifurcations in the system, as well as estimates for the locations of the bifurcation points and the corresponding branches of equilibria which emanate from these bifurcations. For g close to 0, the origin is a stable equilibrium. As g is increased, the origin becomes unstable in a symmetric pitchfork bifurcation at $g = g_0$, at which a new branch of equilibria emerges for each possible division of the inhibitory cells into two synchronized clusters of sizes n_{I_1} and n_{I_2} (the I_1/I_2 branches). We characterize each I_1/I_2 branch by the ratio $\beta = n_{I_1}/n_{I_2}$. We then derive a leading order estimate for the equilibria on each I_1/I_2 branch for g close to g_0 and show that, for large N , these branches are stable for $1 \leq \beta < 2$, but unstable otherwise ($\beta \geq 2$). Furthermore, we show that the equilibria on the I_1/I_2 branches are all unstable for sufficiently large g . Along each I_1/I_2 branch, a Hopf bifurcation creates a branch of periodic orbits, wherein the inhibitory cells maintain their division into the same two synchronized clusters; the frequency of these limit cycles increases with N . We use our estimates for the I_1/I_2 branches to locate these Hopf bifurcations, to leading order, and show that they approach g_0 for large N . All these periodic orbit branches merge at a symmetric pitchfork bifurcation of limit cycles, at some large value of the bifurcation parameter $g = g^*$; for $g > g^*$, there is a single stable limit cycle for which the excitatory population and inhibitory population are each synchronized. See the top figure in Figure 7.1 for a cartoon summary.

We next consider the case where the excitatory cells are broken into clusters of equal size. The connection weights between excitation cells in the same cluster are normalized so that the network is still approximately balanced. In this case, as g is increased from 0, the origin becomes

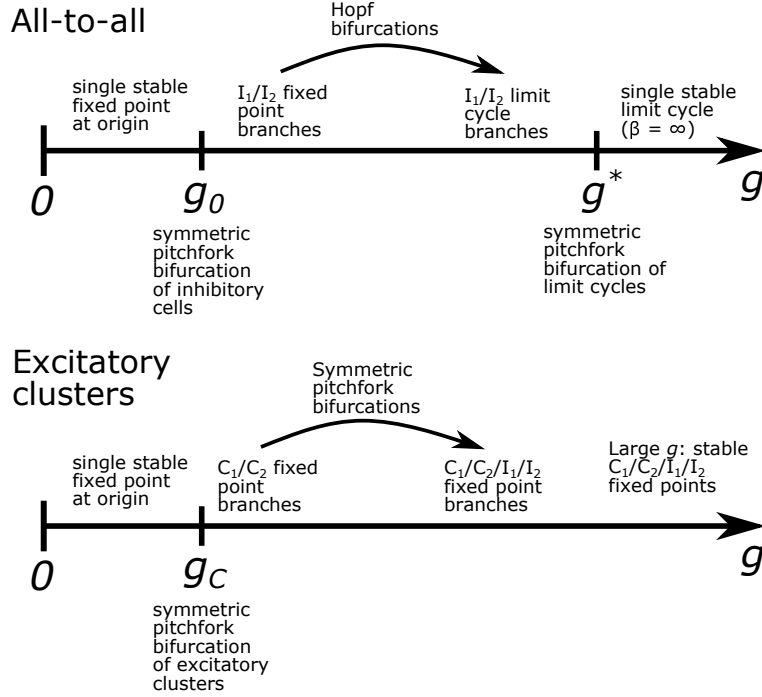


Figure 7.1. Cartoon summary of fixed points, limit cycles, and bifurcations as g increases from 0 for all-to-all connected network (top) and network with excitatory clustering (bottom).

unstable in a symmetric pitchfork bifurcation point at $g = g_C$. In contrast with the previous case, this bifurcation involves the excitatory clusters instead of the inhibitory cells. For $g > g_C$, there is a branch of solutions corresponding to each possible division of the excitatory clusters into synchronized groups of sizes of sizes n_{C_1} and n_{C_2} (the C_1/C_2 branches). We characterize each branch by the ratio $\beta_C = n_{C_1}/n_{C_2}$. Near $g = g_C$, each solution branch is stable for $1 \leq \beta_C < 2$, and is otherwise unstable. Along each C_1/C_2 branch, there is a further symmetric pitchfork bifurcation, in which the inhibitory cells split into two clusters of sizes n_{I_1} and n_{I_2} (with ratio $\beta = n_{I_1}/n_{I_2}$), yielding equilibria in which both the excitatory clusters and the inhibitory cells are split into two groups (the $C_1/C_2/I_1/I_2$ branches). Unlike the previous case, there are no Hopf bifurcations along these branches. For large g , the only branches that remain stable are those for which β_C is close to β , in the precise sense we describe in [subsection 5.5](#); in other words, the excitatory clusters and the inhibitory cells must break up in a similar way. See the bottom figure in [Figure 7.1](#) for a cartoon for a summary. Finally, we briefly consider a network in which the inhibitory cells are clustered, rather than the excitatory cells. Here we find that, as in the case with all-to-all coupling, the origin loses stability in a Hopf bifurcation; however, in contrast to the all-to-all case, the frequency of the resulting limit cycle does not increase with N .

7.1. Relationship to other work. The population-clustered systems we consider in [Sec 4.3-4.6](#) are similar to a simple version of the Wilson–Cowan equations (reviewed in [\[17, 9\]](#)), which can likewise be interpreted in terms of coupled neural populations. Other authors have derived and analyzed similar systems for balanced networks as a mean-field limit from large networks: however, recent examples differ from the current work because of the scaling of the deterministic part of the connectivity matrix. We retain “strong” coupling as a function of system size ($1/\sqrt{N}$) as in [\[32\]](#), vs. “weak” scaling ($1/N$) [\[24, 28, 34\]](#). In [\[24\]](#), for example, connectivity matrices are chosen with entries $J_{ij} \sim N(J/N, \sigma^2/N)$. As $N \rightarrow \infty$, the mean connectivity ($1/N$) goes to zero faster

than the typical random deviation from the mean ($1/\sqrt{N}$); thus outgoing synaptic weights will no longer be single-signed, in violation of Dale’s Law. One consequence of weak scaling seems to be that oscillations are observed at the population but not necessary cell level [21, 6]; in contrast, the limit cycles we describe in subsection 4.5 are observed at both the cell and the population level.

In works that do use strong scaling, the coherent fluctuations that are observed require a perfect orthogonality condition [13, 30] or an external forcing [29] to balance. Furthermore, the nonrandom part of the connectivity matrix is low rank; this is not the case in the current work, in which some examples are low rank but most are not. Contrasting the excitatory clustering with and without self-coupling (section 5 and subsection 5.7), for example, we observe the same pattern of stable fixed points although one is low rank and the other is not.

7.2. Future directions. Future directions include better characterizing the periodic orbits which arise from the Hopf bifurcations in the network with all-to-all coupling case. It may be possible to determine their stability pattern, as well as to locate the bifurcation point at $g = g^*$. Some assumptions about our network can be relaxed; for example the use of the tanh function is not essential to any calculations that don’t explicitly invoke odd symmetry, and could be replaced by another saturating nonlinearity. Another direction includes exploring other network topologies, such as spatial connectivity or hierarchical clustering [33, 15].

Finally, the ultimate goal of these investigations must be to apply these insights to real networks, which will not be perfectly symmetric and which may be modeled by allowing a random perturbation to the connection matrix (i.e. $H \rightarrow H + \epsilon A$). We conjecture that the perturbed system will continue to exhibit fixed points and periodic orbits that are found in the unperturbed system, even when the perturbations are large enough that the spectrum of the connectivity matrix “masks” the underlying symmetry. In our previous study, we found that stable trajectories in the unperturbed all-to-all clustered system accurately predicted which solutions would be observed in the perturbed system [4]. This highlights the importance of determining not only existence but *stability* in the unperturbed system. We look forward to exploring this question in future work.

Appendix A. Solutions along I_1/I_2 branches: detailed calculations.

Here we derive leading order expressions for the equilibria along the I_1/I_2 branches for g close to g_0 . We begin with the simplest case, which is when n_I is even and $\beta = 1$. Taking $x_{I_1} = x_I$, $x_{I_2} = -x_I$, and $x_E = 0$ in (4.6) and simplifying, we obtain the single equation ([4, Eq. 16])

$$-x_I + \frac{\alpha\mu_{EE}}{\sqrt{N}} \tanh(gx_I) = 0,$$

which simplifies to

$$\tanh(gx_I) - g_0x_I = 0. \tag{A.1}$$

Defining $f(x_I) := \tanh(gx_I) - g_0x_I$, $f(0) = 0$, $f'(0) = g - g_0$, and $f(x_I) \rightarrow -\infty$ as $x_I \rightarrow \infty$. When $g > g_0$, $f(x_I)$ is initially increasing, thus it follows from the continuity of f and the intermediate value theorem that (A.1) has a solution with $x_I > 0$ for all $g > g_0$. Furthermore, $x_I \rightarrow 1/g_0$ as $g \rightarrow \infty$.

To obtain an approximation of this solution for g close to g_0 , we expand the LHS of (A.1) in Taylor series about $x_I = 0$ and $g = g_0$ and simplify to get

$$(g - g_0)x_I - \frac{(gx_I)^3}{3} + \frac{2(gx_I)^5}{15} + \mathcal{O}(x_I^7) = 0. \tag{A.2}$$

We note that the remainder term in $(g - g_0)$ is transcendentally small in the sense of [25]. Keeping up to cubic terms in x_I , equation (A.2) simplifies to

$$x_I \left((g - g_0) - \frac{g^3}{3} x_I^2 \right) = 0.$$

Solving for the non-zero solution for x_I results in the expression (4.7). We can obtain a higher-order approximation by keeping up to fifth-order terms in (A.2) to get

$$x_I \left((g - g_0) - \frac{g^3}{3} x_I^2 + \frac{2g^5}{15} x_I^4 \right) = 0,$$

which is x_I multiplied by a quadratic in x_I^2 . To find the nonzero solution for x_I , we solve this quadratic for x_I^2 and take square roots, yielding (4.8).

For $\beta > 1$, as $N \rightarrow \infty$, numerical continuation with the parameter continuation software package AUTO [14] suggests that (4.6) has a solution of the form

$$x_{I_2} = -\beta x_{I_1} + \mathcal{O}\left(\frac{1}{N^2}\right), \quad x_{I_1} = \mathcal{O}\left(\frac{1}{N}\right), \quad x_E = \mathcal{O}\left(\frac{1}{N^2}\right) \quad (\text{A.3})$$

for g close to g_0 . Subtracting the second and third equations in (4.6), we get

$$x_{I_1} - x_{I_2} = \frac{\alpha}{\mu_{EE}\sqrt{N}} (\tanh(gx_{I_1}) - \tanh(gx_{I_2})).$$

Substituting (A.3) as an ansatz, expanding the tanh terms in a Taylor series about $x_{I_1} = 0$ to cubic order, and simplifying, we obtain the formula given in (4.9).

Finally, we show that x_{I_1} and x_{I_2} have opposite signs for all $g > g_0$. Since (4.6) is smooth in (x_E, x_{I_1}, x_{I_2}) and g , the solutions x_{I_1} and x_{I_2} are smooth in g . For g close to g_0 , x_{I_1} and x_{I_2} have opposite signs; if this is not the case for some $g > g_0$, either x_{I_1} or x_{I_2} must pass through 0. We will show that this cannot happen. Suppose $x_{I_1} = 0$ for some $g^* > g_0$. Substituting this into (4.6) and subtracting the second row from the first, we have $x_E = -\frac{\mu_{EE}}{\sqrt{N}} \tanh(g^* x_E)$, which is impossible unless $x_E = 0$. If $x_E = 0$, then $x_{I_2} = -\frac{\mu_{EE}}{\sqrt{N}} \alpha (n_{I_2} - 1) \tanh(g^* x_{I_2})$, which is again impossible unless $x_{I_2} = 0$. Thus $x_{I_1} = 0$ implies $(x_E, x_{I_1}, x_{I_2}) = 0$. This would mean that the I_1/I_2 branch would intersect the zero solution in another bifurcation point at $g^* > g_0$, which we know does not occur, since we have found all bifurcation points of the origin. The case where $x_{I_2} = 0$ for some $g^* > g_0$ is similar.

Appendix B. Stability and bifurcations along I_1/I_2 branches: detailed calculations.

To determine the stability of \mathbf{x}^* for g close to g_0 , we start by computing the eigenvalues of $D\tilde{F}(\mathbf{x}^*)$ corresponding to λ_{I_1} and λ_{I_2} . Substituting (4.9) for x_{I_1} , using the Taylor series expansion $\text{sech}^2 x = 1 - x^2 + \mathcal{O}(x^4)$, and simplifying, the eigenvalue $\lambda_{I_1}^*(g)$ of $D\tilde{F}(\mathbf{x}^*)$ is located at

$$\lambda_{I_1}^*(g) = \frac{g - g_0}{g} \left(1 - \frac{3}{1 - \beta + \beta^2} \right) + \mathcal{O}\left(\frac{1}{N^2}\right) \quad g > g_0,$$

which is negative for $1 \leq \beta < 2$ and positive for $\beta > 2$. Similarly, the eigenvalue $\lambda_{I_2}^*(g)$ of $D\tilde{F}(\mathbf{x}^*)$ corresponding to λ_{I_2} is located at

$$\lambda_{I_2}^*(g) = \frac{g - g_0}{g} \left(1 - \frac{3\beta^2}{1 - \beta + \beta^2} \right) + \mathcal{O}\left(\frac{1}{N^2}\right) \quad g > g_0,$$

which is negative for $\beta > 1/2$ and thus does not affect stability.

It remains to find leading order expressions for the eigenvalues of $H_3(\mathbf{x})$. When $\mathbf{x} = 0$, the matrix $H_3(0)$ has a single eigenvalue at λ_I and a complex conjugate pair of eigenvalues $\lambda_0 \pm \omega_0$, where these are defined at the beginning of section 4. These do not depend on β . For \mathbf{x} small but nonzero, we use a perturbation method to approximate the eigenvalues of $H_3(\mathbf{x})$. We substitute

the expressions (A.3) into characteristic polynomial for $H_3(\mathbf{x})$, keeping only terms of up to order $1/N$, so that the leading order expression only involves x_{I_1} . We then use the Taylor expansion $\text{sech}^2(gx_{I_1}) = 1 - (gx_{I_1})^2 + \mathcal{O}(x_{I_1}^4)$, keeping only terms up to quadratic order. For each eigenvalue λ of $H_3(\mathbf{x})$, we use a power series ansatz

$$\lambda + \epsilon x_{I_1}^2 + \mathcal{O}(x_{I_1})^4. \quad (\text{B.1})$$

We substitute this ansatz into the characteristic polynomial for $H_3(\mathbf{x})$ and solve for ϵ by matching the coefficients of $x_{I_1}^2$. (This computation, and the remaining computations in this section, were performed with the aid of Wolfram Mathematica). Using this method for $\lambda = \lambda_I$, $H_3(\mathbf{x}^*)$ has a real eigenvalue located at

$$\lambda_I = \alpha\mu_{EE} (1 - (1 - \beta + \beta^2)g^2 x_{I_1}^2) + \mathcal{O}\left(\frac{1}{N^2}\right).$$

Substituting the estimate (4.9) for x_{I_1} and simplifying, the eigenvalue $\lambda_I^*(g)$ of $J_3(\mathbf{x})$ corresponding to λ_I is located at

$$\lambda_I^*(g) = \frac{\alpha\mu_{EE}g}{\sqrt{N}} \left(1 - \frac{3(g-g_0)}{g}\right) - 1 = -2 \left(\frac{g-g_0}{g_0}\right) + \mathcal{O}\left(\frac{1}{N^2}\right) \quad g \geq g_0,$$

which is always negative, and thus does not affect stability.

Finally, we use this method to locate the eigenvalue of $H_3(\mathbf{x})$ corresponding to $\lambda_0 \pm \omega_0$. In doing so, we will find a Hopf bifurcation on each I_1/I_2 branch. $H_3(\mathbf{x})$ has a complex conjugate pair of eigenvalues, where the real part is given by

$$\lambda_0(g, \beta) = \frac{\mu_{EE}}{2} (\alpha - 1 + \alpha\beta g^2 (n_I - 1)x_{I_1}^2) + \mathcal{O}\left(\frac{1}{N}\right). \quad (\text{B.2})$$

We can get more accurate approximations for $\lambda(g, \beta)$ by taking higher powers of x_{I_1} in our power series ansatz (B.1). For example, when $\beta = 1$, we can obtain the fourth-order approximation

$$\lambda_0(g, 1) = \frac{\mu_{EE}}{2} \left(\alpha - 1 + \alpha g^2 (n_I - 1)x_{I_1}^2 - \frac{2}{3}\alpha g^4 (n_I - 1)x_{I_1}^4 \right) + \mathcal{O}\left(\frac{1}{N^2}\right).$$

Similar fourth-order approximations can be obtained when $\beta > 1$, but the resulting coefficient of $x_{I_1}^4$ is significantly more complicated. Substituting (4.9) for x_{I_1} and simplifying, $J_3(\mathbf{x})$ has a complex conjugate pair of eigenvalues $\lambda_0^*(g) \pm i\omega_0^*(g)$, where

$$\lambda_0^*(g, \beta) = \frac{\mu_{EE}g}{2\sqrt{N}} \left[\alpha - 1 + \alpha\beta(n_I - 1) \frac{3(g-g_0)}{(1-\beta+\beta^2)g} \right] - 1 + \mathcal{O}\left(\frac{1}{N}\right). \quad (\text{B.3})$$

To locate the Hopf bifurcation on each I_1/I_2 branch, which occurs when the complex pair of eigenvalues crosses the imaginary axis, we solve $\lambda_0^*(g, \beta) = 0$ for g , substitute $g_0 = \sqrt{N}/\alpha\mu_{EE}$, and simplify to obtain the expression in (4.12).

Appendix C. Proof of Proposition 4.3.

First, we show that that (4.14) has no fixed points other than the origin. To do this, we make the change of variables $(y_1, y_2) = (\tanh(gx_1), \tanh(gx_2))$, and note that it is equivalent to show that the system of equations

$$\begin{aligned} g_1(y_1, y_2) &:= -\frac{1}{g} \tanh^{-1}(y_1) + \frac{\mu_{EE}}{\sqrt{N}} ((n_E - 1)y_1 - \alpha n_I y_2) = 0 \\ g_2(y_1, y_2) &:= -\frac{1}{g} \tanh^{-1}(y_2) + \frac{\mu_{EE}}{\sqrt{N}} (n_E y_1 - \alpha(n_I - 1)y_2) = 0 \end{aligned} \quad (\text{C.1})$$

has no solution other than $(y_1, y_2) = (0, 0)$. The first equation $g_1(y_1, y_2) = 0$ is satisfied when

$$y_2 = y_2^*(y_1) := \frac{g\mu_{EE}(n_E - 1)y_1 - \sqrt{N} \tanh^{-1}(y_1)}{\alpha g\mu_{EE}n_I}. \quad (\text{C.2})$$

To show that (C.1) has no solutions other than the origin, we substitute (C.2) into $g_2(y_1, y_2)$ to get

$$\begin{aligned} g_2(y_1, y_2^*(y_1)) &= \frac{\mu_{EE}(n_E + n_I - 1)y_1}{n_I\sqrt{N}} + \frac{n_I - 1}{gn_I} \tanh^{-1}(y_1) \\ &+ \frac{1}{g} \tanh^{-1} \left(\frac{\sqrt{N} \tanh^{-1}(y_1) - g\mu_{EE}(n_E - 1)y_1}{\alpha g\mu_{EE}n_I} \right). \end{aligned} \quad (\text{C.3})$$

We will show that $g_2(y_1, y_2^*(y_1)) > 0$ for $y_1 > 0$. Since $g_2(y_1, y_2^*(y_1))$ is an odd function in y_1 , this will imply that $g_2(y_1, y_2^*(y_1)) < 0$ for $y_1 < 0$, from which the desired result will follow. Since $\tanh^{-1} y_1 \geq y_1$ for $y_1 \geq 0$, it suffices to show that

$$\begin{aligned} h(y_1) &:= \frac{\mu_{EE}(n_E + n_I - 1)y_1}{n_I\sqrt{N}} + \frac{n_I - 1}{gn_I} \tanh^{-1}(y_1) \\ &+ \frac{1}{g} \tanh^{-1} \left(\frac{\sqrt{N} \tanh^{-1}(y_1) - g\mu_{EE}(n_E - 1)y_1}{\alpha g\mu_{EE}n_I} \right) > 0 \end{aligned} \quad (\text{C.4})$$

for $y_1 > 0$. Since $h(0) = 0$, we will show that $h'(0) > 0$ for $y_1 > 0$. Computing the derivative with the assistance of Mathematica,

$$\begin{aligned} h'(y_1) &= \frac{(N-1)\mu_{EE}}{(1-f)N^{3/2}} + \frac{1}{g(1-y_1^2)} - \frac{f\mu_{EE}N(g\mu_{EE}(fN-1) - \sqrt{N})}{f^2g^2\mu_{EE}^2N^2 - (\sqrt{N} + g\mu_{EE}(1-fN))^2y_1^2} \\ &\geq \frac{(N-1)\mu_{EE}}{(1-f)N^{3/2}} + \frac{1}{g(1-y_1^2)} - \frac{1}{g \left(1 - \left(\frac{fN-1}{fN} \right)^2 y_1^2 \right)} \\ &\geq \frac{(N-1)\mu_{EE}}{(1-f)N^{3/2}} > 0. \end{aligned}$$

We have therefore shown that (4.14) has no fixed points other than the origin.

The Linearization of (4.14) about the origin is the 2×2 matrix

$$J = \frac{g\mu_{EE}}{\sqrt{N}} \begin{bmatrix} n_E - 1 & -\alpha n_I \\ n_E & -\alpha(n_I - 1) \end{bmatrix} - I_2,$$

which has a complex conjugate pair of eigenvalues $\frac{g}{\sqrt{N}}(\lambda_0 \pm i\omega_0) - 1$, where λ_0 and ω_0 are defined in section 4. This pair crosses through the imaginary axis at $g = g_H$, where g_H is defined by (4.2), leading to a Hopf bifurcation in the reduced system (4.14), and the origin is repelling for $g > g_H$. To show there is a limit cycle for all $g > g_H$, we use the Poincaré-Bendixson theorem [11, Chapter 16]. For a trapping region, we draw a square around the origin with corners $(-a, -a)$ and (a, a) . On the line $x = a$, for a large,

$$\dot{x} \leq -a + \frac{2n_E}{\sqrt{N}} = -a + 2f\sqrt{N},$$

which can be made negative by taking a sufficiently large. Similarly, we can take a sufficiently large so that the vector field defined by (4.14) points inward at all points on the square (Figure C.1).

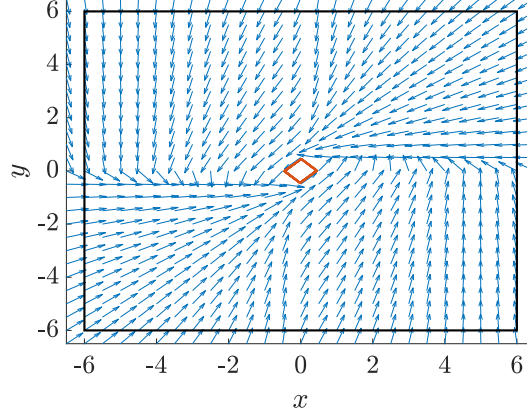


Figure C.1. Slope fields for (4.14), with a small limit cycle visible in center. Slope field points inward on black box, which is the trapping region for the Poincaré-Bendixson theorem. Parameters: $N = 20$, $g = 5$, $\alpha = 4$, and $\mu_{EE} = 0.7$.

$\text{sgn}(\hat{x}_E, \hat{x}_{I_1}, \hat{x}_{I_2})$	$\frac{\sqrt{N}}{\mu_{EE}} \hat{x}_E$	$\frac{\sqrt{N}}{\mu_{EE}} \hat{x}_{I_1}$	$\frac{\sqrt{N}}{\mu_{EE}} \hat{x}_{I_2}$
(1, 1, 1)	$-1 < 0$	α	α
(1, -1, -1)	$2\alpha n_I - 1$	$\alpha(2n_I - 1) > 0$	$\alpha(2n_I - 1) > 0$
(1, 1, -1)	$2\alpha n_{I_2} - 1$	$\alpha(2n_{I_2} + 1)$	$\alpha(2n_{I_2} - 1) > 0$
(1, -1, 1)	$2\alpha n_{I_1} - 1$	$\alpha(2n_{I_1} - 1) > 0$	$\alpha(2n_{I_1} + 1) > 0$

Table D.1

Sign table showing that all solutions for nonzero $(\hat{x}_E, \hat{x}_{I_1}, \hat{x}_{I_2})$ are inconsistent.

Since the origin is repelling for $g > g_H$ and is the only fixed point of the system, it follows from the Poincaré-Bendixson theorem that there is a limit cycle surrounding the origin for $g > g_H$. We note that although the limit cycle from Proposition 4.3 is stable in the two-dimensional system (4.14), the theorem says nothing about its stability in the full system (2.1).

Appendix D. Stability of the I_1/I_2 branch for large g : detailed calculations .

Here we prove our assertion, made in subsection 4.6, that $x_E \rightarrow 0$ as $g \rightarrow \infty$ along any I_1/I_2 solution branch. Suppose, instead, that $x_E \rightarrow \hat{x}_E \neq 0$ as $g \rightarrow \infty$. Without loss of generality, we can take $\hat{x}_E > 0$, since by odd symmetry of (2.1), there will be a corresponding solution with $\hat{x}_E < 0$. This implies that $\tanh x_E \rightarrow 1$. There are four cases to consider:

- Case 1: $x_{I_1} \rightarrow \hat{x}_{I_1} \neq 0$ and $x_{I_2} \rightarrow \hat{x}_{I_2} \neq 0$.
- Case 2: $x_{I_1} \rightarrow \hat{x}_{I_1} \neq 0$ and $x_{I_2} \rightarrow 0$.
- Case 3: $x_{I_1} \rightarrow 0$ and $x_{I_2} \rightarrow \hat{x}_{I_2} \neq 0$.
- Case 4: $x_{I_1} \rightarrow 0$ and $x_{I_2} \rightarrow 0$.

The computations to follow were done with the assistance of Wolfram Mathematica. For Case 1, $\tanh(gx_{I_1}) \rightarrow \pm 1$ and $\tanh(gx_{I_2}) \rightarrow \pm 1$. We can then use (4.6) to solve for $(\hat{x}_E, \hat{x}_{I_1}, \hat{x}_{I_2})$. The signs of these solutions are all inconsistent, as we can see in Table D.1.

For Case 2, if $\tanh(g\hat{x}_{I_2}) \rightarrow 0$, the solution $(\hat{x}_E, \hat{x}_{I_1}, \hat{x}_{I_2})$ from (4.6) is inconsistent using the same argument as in Case 1. The only remaining possibility is $\tanh(g\hat{x}_{I_2}) \rightarrow \hat{y}_{I_2}$, where $0 < |\hat{y}_{I_2}| < 1$. In

the limit $g \rightarrow \infty$, (4.6) becomes

$$\begin{bmatrix} \hat{x}_E \\ \hat{x}_{I_1} \\ 0 \end{bmatrix} = \frac{\mu_{EE}}{\sqrt{N}} \begin{bmatrix} (\alpha n_I - 1) & -\alpha \frac{\beta}{\beta+1} n_I & -\alpha \frac{1}{\beta+1} n_I \\ \alpha n_I & -\alpha \left(\frac{\beta}{\beta+1} n_I - 1 \right) & -\alpha \frac{1}{\beta+1} n_I \\ \alpha n_I & -\alpha \frac{\beta}{\beta+1} n_I & -\alpha \left(\frac{1}{\beta+1} n_I - 1 \right) \end{bmatrix} \begin{bmatrix} 1 \\ \pm 1 \\ \hat{y}_{I_2} \end{bmatrix}.$$

The consistency condition (from the third row) can only be satisfied if $\hat{y}_{I_2} = \frac{n_I}{n_I - (\beta+1)} > 1$ (for $\hat{x}_{I_1} > 0$) or $\hat{y}_{I_2} = \frac{n_I(1+2\beta)}{n_I - (\beta+1)} > 1$ (for $\hat{x}_{I_1} < 0$), both of which are impossible. Case 3 is similar.

For Case 4, if $\tanh(g\hat{x}_{I_1}) \rightarrow 0$ or $\tanh(g\hat{x}_{I_2}) \rightarrow 0$, the solution $(\hat{x}_E, \hat{x}_{I_1}, \hat{x}_{I_2})$ from (4.6) is inconsistent using the same argument as in Case 1. The remaining possibility is $\tanh(g\hat{x}_{I_1}) \rightarrow \hat{y}_{I_1}$ and $\tanh(g\hat{x}_{I_2}) \rightarrow \hat{y}_{I_2}$, where $0 < |\hat{y}_{I_1}|, |\hat{y}_{I_2}| < 1$. In the limit $g \rightarrow \infty$, (4.6) becomes

$$\begin{bmatrix} \hat{x}_E \\ 0 \\ 0 \end{bmatrix} = \frac{\mu_{EE}}{\sqrt{N}} \begin{bmatrix} (\alpha n_I - 1) & -\alpha \frac{\beta}{\beta+1} n_I & -\alpha \frac{1}{\beta+1} n_I \\ \alpha n_I & -\alpha \left(\frac{\beta}{\beta+1} n_I - 1 \right) & -\alpha \frac{1}{\beta+1} n_I \\ \alpha n_I & -\alpha \frac{\beta}{\beta+1} n_I & -\alpha \left(\frac{1}{\beta+1} n_I - 1 \right) \end{bmatrix} \begin{bmatrix} 1 \\ \hat{y}_{I_1} \\ \hat{y}_{I_2} \end{bmatrix}.$$

The consistency conditions (from the second and third rows) can only be satisfied if $\hat{y}_{I_1} = \hat{y}_{I_2} = \frac{n_I}{n_I - 1} > 1$, which is impossible.

Appendix E. Stability and bifurcations along C_1/C_2 branch: detailed calculations.

Following the procedure in subsection 4.4 and Appendix B, we substitute the expressions from (5.5) into the the formulas for the eigenvalues in Proposition 5.1 and simplify to obtain leading order expressions for the corresponding eigenvalues of $D\tilde{F}(\mathbf{x}^*)$

$$\begin{aligned} \lambda_{C_1}^*(g) &= \frac{g - g_C}{g} \left(1 - \frac{3}{1 - \beta_C + \beta_C^2} \right) \\ \lambda_{C_2}^*(g) &= \frac{g - g_C}{g} \left(1 - \frac{3\beta_C^3}{1 - \beta_C + \beta_C^2} \right) \\ \lambda_I^*(g) &= \frac{\alpha\mu g}{\sqrt{N}} - 1. \end{aligned} \tag{E.1}$$

$\lambda_{C_1}^*(g)$ is negative for $1 \leq \beta_C < 2$ and positive for $\beta_C > 2$; $\lambda_{C_2}^*(g)$ is negative for $\beta_C > 1/2$; and $\lambda_I^*(g)$ is negative for all β_C for N sufficiently large.

It remains to find leading order expressions for the eigenvalues of $H_3(\mathbf{x})$, given by (5.7). When $\mathbf{x} = 0$, the matrix $H_3(0)$ has a single eigenvalue at λ_C and a complex conjugate pair of eigenvalues $\lambda_0 \pm i\omega_0$, where these are defined at the beginning of section 5. Using the same asymptotic procedure as in subsection 4.4 and Appendix B, $H_3(\mathbf{x}^*)$ has a real eigenvalue corresponding to λ_C located at

$$\lambda_C(\mathbf{x}^*) = (p - 1)n_C\mu \left(1 - (1 - \beta_C + \beta_C^2)g^2x_{E_1}^2 \right) + \mathcal{O}\left(\frac{1}{N^2}\right).$$

Substituting the estimate (5.5) for x_{E_1} and simplifying, the eigenvalue $\lambda_C^*(g)$ of $J_3(\mathbf{x}^*)$ corresponding to λ_C is located, to leading order, at

$$\lambda_C^*(g) = -2 \left(\frac{g - g_C}{g_C} \right),$$

for g close to g_C . Since this eigenvalue is always negative, it will not affect stability. Similarly, $H_3(\mathbf{x})$ has a complex conjugate pair of eigenvalues $\lambda_0 + i\omega_0$, where the real part is given by

$$\lambda_0(g, \beta_C) = \frac{\mu}{2} [(\alpha - n_C) - \beta_C g^2 n_C (p - 1) x_{E_1}^2]$$

to leading order, for g close to g_C . Since we are taking $n_C \geq \alpha$, this is always negative for g close to g_C .

Appendix F. C_1/C_2 branches for large g : detailed calculations. Here we provide details of the behavior of solutions on the C_1/C_2 branch as g becomes large. We claim there are two patterns for the limiting behavior on the C_1/C_2 branches, which depend on whether $\beta_C < \beta_C^*$ or $\beta_C > \beta_C^*$, for some critical value β_C^* , which we will determine below. These were illustrated in [Figure 5.3](#).

- Case 1: ($1 < \beta_C < \beta_C^*$) $x_{E_1} \rightarrow \hat{x}_{E_1} > 0$ and $x_{E_2} \rightarrow \hat{x}_{E_2} < 0$.
- Case 2: ($\beta_C > \beta_C^*$) $x_{E_1} \rightarrow 0$ with $\tanh(gx_{E_1}) \rightarrow \hat{y}_{E_1} \neq 0$, and $x_{E_2} \rightarrow \hat{x}_{E_2} < 0$.

For Case 1, since $\tanh(gx_{E_1}) \rightarrow 1$ and $\tanh(gx_{E_2}) \rightarrow -1$, we can solve for \hat{y}_I using row 3 of [\(5.4\)](#) to get

$$\hat{y}_I = \frac{\beta_C - 1}{\beta_C + 1} \frac{pn_C}{pn_C - \alpha}, \quad (\text{F.1})$$

from which it follows that

$$x_I \rightarrow \frac{1}{g} \tanh^{-1} \left(\frac{\beta_C - 1}{\beta_C + 1} \frac{pn_C}{pn_C - \alpha} \right) \text{ as } g \rightarrow \infty. \quad (\text{F.2})$$

Using [\(F.1\)](#) with rows 1 and 2 of [\(5.4\)](#),

$$\begin{aligned} \hat{x}_{E_1} &= \frac{\mu}{\sqrt{N}} \left((p-1)n_C - \frac{\beta_C - 1}{\beta_C + 1} \frac{p^2 n_C^2}{pn_C - \alpha} \right) \\ \hat{x}_{E_2} &= \frac{\mu}{\sqrt{N}} \left(-(p-1)n_C - \frac{\beta_C - 1}{\beta_C + 1} \frac{p^2 n_C^2}{pn_C - \alpha} \right), \end{aligned} \quad (\text{F.3})$$

which reduce to [\(5.9\)](#) when $\beta_C = 1$. Since $n_C p = fN \rightarrow \infty$ as $N \rightarrow \infty$, this simplifies to

$$\begin{aligned} x_{E_1} &\rightarrow \frac{\mu}{\sqrt{N}} \left((p-1)n_C - \frac{\beta_C - 1}{\beta_C + 1} pn_C \right) \\ x_{E_2} &\rightarrow \frac{\mu}{\sqrt{N}} \left(-(p-1)n_C - \frac{\beta_C - 1}{\beta_C + 1} pn_C \right) \\ x_I &\rightarrow \frac{1}{g} \tanh^{-1} \left(\frac{\beta_C - 1}{\beta_C + 1} \right) \end{aligned} \quad (\text{F.4})$$

as $g, N \rightarrow \infty$. For [\(F.3\)](#) to be valid, the consistency conditions $\hat{x}_{E_1} > 0$ and $\hat{x}_{E_2} < 0$ must be satisfied. Since $\hat{x}_{E_2} < 0$ always holds, [\(F.3\)](#) is consistent as long as

$$(p-1)n_C - \frac{\beta_C - 1}{\beta_C + 1} \frac{p^2 n_C^2}{pn_C - \alpha} > 0. \quad (\text{F.5})$$

Solving for β_C , this results in the condition $\beta_C < \beta_C^*$, where β_C^* is defined in [5.10](#).

For Case 2, we can solve for \hat{y}_{E_1} and \hat{y}_I using rows 2 and 3 of [\(5.4\)](#) to get

$$\begin{aligned} \hat{y}_{E_1} &= \frac{n_C p^2}{\alpha(1 + \beta_C)(p-1) + n_C p(1 + \beta_C - p)} \\ \hat{y}_I &= \frac{n_C p(p-1)}{\alpha(1 + \beta_C)(p-1) + n_C p(1 + \beta_C - p)}, \end{aligned} \quad (\text{F.6})$$

from which it follows that

$$\begin{aligned}
x_{E_1} &\rightarrow \frac{1}{g} \tanh^{-1} \left(\frac{n_C p^2}{\alpha(1 + \beta_C)(p - 1) + n_C p(1 + \beta_C - p)} \right) \\
x_{E_2} &\rightarrow \frac{\mu}{\sqrt{N}} \left(-(p - 1)n_C - \frac{n_C^2 p^2 (p - 1)}{\alpha(1 + \beta_C)(p - 1) + n_C p(1 + \beta_C - p)} \right) \\
x_I &\rightarrow \frac{1}{g} \tanh^{-1} \left(\frac{n_C p (p - 1)}{\alpha(1 + \beta_C)(p - 1) + n_C p(1 + \beta_C - p)} \right).
\end{aligned} \tag{F.7}$$

as $g \rightarrow \infty$. We note that for $\beta_C > \beta_C^*$, we cannot take $N \rightarrow \infty$ with n_C held fixed, since for sufficiently large N we will always have $\beta_C < \beta_C^*$.

Appendix G. Stable excitatory clusters for large g : detailed calculations. We begin with the ansatz (suggested by numerical continuation) that as $g \rightarrow \infty$, $(x_{E_1}, x_{E_2}, x_{I_1}, x_{I_2}) \rightarrow (\hat{x}_{E_1}, \hat{x}_{E_2}, \hat{x}_{I_1}, \hat{x}_{I_2})$, where $\hat{x}_{E_1}, \hat{x}_{I_1} > 0$ and $\hat{x}_{E_2}, \hat{x}_{I_2} < 0$. With these assumptions, equation (5.12) reduces to

$$\begin{aligned}
\hat{x}_{E_1} &= \frac{\mu}{\sqrt{N}} \left[(p - 1)n_C - \alpha \frac{\beta - 1}{\beta + 1} n_I \right] \\
\hat{x}_{E_2} &= \frac{\mu}{\sqrt{N}} \left[-(p - 1)n_C - \alpha \frac{\beta - 1}{\beta + 1} n_I \right] \\
\hat{x}_{I_1} &= \frac{\mu}{\sqrt{N}} \left[\frac{\beta_C - 1}{\beta_C + 1} p n_C - \alpha \left(\frac{\beta - 1}{\beta + 1} n_I - 1 \right) \right] \\
\hat{x}_{I_2} &= \frac{\mu}{\sqrt{N}} \left[\frac{\beta_C - 1}{\beta_C + 1} p n_C - \alpha \left(\frac{\beta - 1}{\beta + 1} n_I + 1 \right) \right],
\end{aligned} \tag{G.1}$$

since $\tanh(gx_{E_1}), \tanh(gx_{I_1}) \rightarrow 1$ and $\tanh(gx_{E_2}), \tanh(gx_{I_2}) \rightarrow -1$ as $g \rightarrow \infty$. Equation (G.1) gives the limiting solutions $(\hat{x}_{E_1}, \hat{x}_{E_2}, \hat{x}_{I_1}, \hat{x}_{I_2})$ as long as the consistency conditions $\hat{x}_{E_1}, \hat{x}_{I_1} > 0$ and $\hat{x}_{E_2}, \hat{x}_{I_2} < 0$ are satisfied. Since $\mu > 0$, the consistency conditions reduce to

$$\begin{aligned}
(p - 1)n_C - \alpha \frac{\beta - 1}{\beta + 1} n_I &> 0 \\
-(p - 1)n_C - \alpha \frac{\beta - 1}{\beta + 1} n_I &< 0 \\
\frac{\beta_C - 1}{\beta_C + 1} p n_C - \alpha \left(\frac{\beta - 1}{\beta + 1} n_I - 1 \right) &> 0 \\
\frac{\beta_C - 1}{\beta_C + 1} p n_C - \alpha \left(\frac{\beta - 1}{\beta + 1} n_I + 1 \right) &< 0.
\end{aligned} \tag{G.2}$$

The first pair of inequalities in (G.2) is satisfied if and only if

$$\left| \frac{\beta - 1}{\beta + 1} \right| < \frac{(p - 1)n_C}{\alpha n_I} = 1 - \frac{1}{p},$$

where we used the fact that $n_C p = n_E = \alpha n_I$. Since we are taking $\beta \geq 1$, this simplifies to $1 \leq \beta < 2p$. Similarly, the second pair of inequalities in (G.2) is satisfied if and only if

$$\alpha \left(\frac{\beta - 1}{\beta + 1} n_I - 1 \right) < \frac{\beta_C - 1}{\beta_C + 1} p n_C < \alpha \left(\frac{\beta - 1}{\beta + 1} n_I + 1 \right),$$

which simplifies to (5.13).

REFERENCES

- [1] Y. AHMADIAN, F. FUMAROLA, AND K. D. MILLER, *Properties of networks with partially structured and partially random connectivity*, Physical Review E, 91 (2015), p. 012820.
- [2] J. ALJADIEFF, M. STERN, AND T. SHARPEE, *Transition to chaos in random networks with cell-type-specific connectivity*, Physical Review Letters, 114 (2015), p. 088101.
- [3] Z. BAI, *Circular law*, Annals of Probability, 25 (1997), pp. 494–529.
- [4] A. K. BARREIRO, KUTZ, J. NATHAN, AND SHLIZERMAN, ELI, *Symmetries Constrain Dynamics in a Family of Balanced Neural Networks*, Journal of Mathematical Neuroscience, 7 (2017), p. 28, <https://doi.org/10.1186/s13408-017-0052-6>.
- [5] M. BEIRAN, A. DUBREUIL, A. VALENTE, F. MASTROGIUSEPPE, AND S. OSTOJIC, *Shaping dynamics with multiple populations in low-rank recurrent networks*, Neural Computation, 33 (2021), pp. 1572–1615.
- [6] N. BRUNAL AND V. HAKIM, *Fast global oscillations in networks of integrate-and-fire neurons with low firing rates*, Neural Computation, 11 (1999), pp. 1621–1671.
- [7] D. BUXHOEVEDEN AND M. CASANOVA, *The minicolumn hypothesis in neuroscience*, Brain, 125 (2002), pp. 935–951.
- [8] W. CHAISANGMONGKON, S. K. SWAMINATHAN, D. J. FREEDMAN, AND X. J. WANG, *Computing by robust transience: How the fronto-parietal network performs sequential, category-based decisions*, Neuron, 93 (2017), pp. 1504–1517.
- [9] C. C. CHOW AND Y. KARIMIPANAH, *Before and beyond the wilson-cowan equations*, Journal of neurophysiology, 123 (2020), pp. 1645–1656, <https://doi.org/10.1152/jn.00404.2019>.
- [10] G. CICOGNA, *Symmetry breakdown from bifurcation*, Lett. Nuovo Cimento (2), 31 (1981), pp. 600–602.
- [11] E. A. CODDINGTON AND N. LEVINSON, *Theory of ordinary differential equations*, McGraw-Hill New York, 1955.
- [12] R. DARSHAN, C. V. VREESWIJK, AND D. HANSEL, *Strength of correlations in strongly recurrent neuronal networks*, Phys. Rev. X, 8 (2018).
- [13] L. G. DEL MOLINO, K. PAKDAMAN, J. TOUBOUL, AND G. WAINRIB, *Synchronization in random balanced networks*, Physical Review E, 88 (2013), p. 042824.
- [14] E. J. DOEDEL, T. F. FAIRGRIEVE, B. SANDSTEDTE, A. R. CHAMPNEYS, Y. A. KUZNETSOV, AND X. WANG, *AUTO-07P: Continuation and bifurcation software for ordinary differential equations*, tech. report, 2007.
- [15] C. EBSCH AND R. ROSENBAUM, *Imbalanced amplification: A mechanism of amplification and suppression from local imbalance of excitation and inhibition in cortical circuits*, PLoS computational biology, 14 (2018), p. e1006048.
- [16] A. ECKER, P. BERENS, R. J. COTTON, M. SUBRAMANIYAN, G. H. DENFIELD, C. R. CADWELL, S. M. SMIRNAKIS, M. BETHGE, AND A. S. TOLIAS, *State dependence of noise correlations in macaque primary visual cortex*, Neuron, 82 (2014), pp. 235–248.
- [17] G. ERMENTROUT AND D. TERMAN, *Foundations of Mathematical Neuroscience*, Springer, 2010.
- [18] J. A. GALLEGO, P. M. G., S. N. NAUFEL, C. ETHIER, S. A. SOLLA, AND L. E. MILLER, *Cortical population activity within a preserved neural manifold underlies multiple motor behaviors*, Nature Communications, 9 (2018), pp. 1–13.
- [19] J. A. GALLEGO, M. G. PERICH, R. H. CHOWDHURY, S. A. SOLLA, AND L. E. MILLER, *Long-term stability of cortical population dynamics underlying consistent behavior*, Nature neuroscience, 23 (2020), pp. 260–270.
- [20] P. GAO, S. GANGULI, F. P. BATTAGLIA, AND M. J. SCHNITZER, *On simplicity and complexity in the brave new world of large-scale neuroscience*, Current Opinion in Neurobiology, 32 (2015), pp. 148–155.
- [21] I. GINZBURG AND H. SOMPOLINSKY, *Theory of correlations in stochastic neural networks*, Physical Review E, 50 (1994), pp. 3171–3191.
- [22] V. GIRKO, *Circular law*, Theory Probab. Appl., 29 (1985), pp. 694–706.
- [23] M. GOLUBITSKY, I. STEWART, AND D. SCHAEFFER, *Singularities and Groups in Bifurcation Theory, Vol II*, Springer-Verlag, 1988.
- [24] G. HERMANN AND J. TOUBOUL, *Heterogeneous connections induce oscillations in large-scale networks*, Physical Review Letters, 109 (2012), p. 018702.
- [25] M. H. HOLMES, *Introduction to Perturbation Methods*, Texts in Applied Mathematics, Springer, 2nd ed. 2013 ed., 2012.
- [26] R. B. HOYLE, *Pattern formation : an introduction to methods*, Cambridge texts in applied mathematics, Cambridge University, Cambridge, 2006.
- [27] C. HUANG, D. A. RUFF, R. PYLE, R. ROSENBAUM, M. R. COHEN, AND B. DOIRON, *Circuit models of low-dimensional shared variability in cortical networks*, Neuron, 101 (2019), pp. 337–348.
- [28] J. KADMON AND H. SOMPOLINSKY, *Transition to chaos in random neuronal networks*, Physical Review X, 5 (2015), p. 041030.
- [29] I. LANDAU AND H. SOMPOLINSKY, *Macroscopic fluctuations emerge in balanced networks with incomplete re-*

- current alignment*, Physical Review Research, 3 (2021).
- [30] I. D. LANDAU AND H. SOMPOLINSKY, *Coherent chaos in a recurrent neural network with structured connectivity*, PLoS Comput. Biol., 14 (2018).
 - [31] D. MUIR AND T. MRSIC-FLOGEL, *Eigenspectrum bounds for semirandom matrices with modular and spatial structure for neural networks*, Physical Review E, 91 (2015), p. 042808.
 - [32] K. RAJAN AND L. ABBOTT, *Eigenvalue spectra of random matrices for neural networks*, Physical Review Letters, 97 (2006), p. 188104.
 - [33] R. ROSENBAUM, M. A. SMITH, A. KOHN, J. E. RUBIN, AND B. DOIRON, *The spatial structure of correlated neuronal variability*, Nature Neuroscience, 20 (2017), pp. 107–114.
 - [34] F. SCHUESSLER, A. DUBREUIL, F. MASTROGIUSEPPE, S. OSTOJIC, AND O. BARAK, *Dynamics of random recurrent networks with correlated low-rank structure*, Phys. Rev. Research, 2 (2020).
 - [35] H. SOMPOLINSKY, A. CRISANTI, AND H. SOMMERS, *Chaos in random neural networks*, Physical Review Letters, 61 (1988), pp. 259–262.
 - [36] J. WANG, D. NARAIN, E. A. HOSSEINI, AND M. JAZAYERI, *Flexible timing by temporal scaling of cortical responses*, Nature Neuroscience, 21 (2018), pp. 102–112.
 - [37] Y. WEI, *Eigenvalue spectra of asymmetric random matrices for multicomponent neural networks*, Physical Review E, 85 (2012), p. 066116.